Influence of carbon nanotubes and cement reduction on the bond strength of steel bars in concrete: An experimental investigation

E.D. Reis, Fabrice Gatuingt, F.S.J. Poggiali, A.C.S. Bezerra

Influence of carbon nanotubes and cement reduction on the bond strength of steel bars in concrete: an experimental investigation

E. D. Reis[a,b], F. Gatuingt[b], F. S. J. Poggiali[a], A. C. S. Bezerra[c]

[a] Federal Center for Technological Education of Minas Gerais, Dept. of Civil Engineering, Belo Horizonte, Brazil.
[b] Université Paris-Saclay, CentraleSupélec, ENS Paris-Saclay, CNRS, LMPS – Laboratoire de Mécanique Paris-Saclay, Gif-sur-Yvette, France.
[c] Federal Center for Technological Education of Minas Gerais, Dept. of Transport Engineering, Belo Horizonte, Brazil.

Corresponding author: Elvys Dias Reis
elvysreis@yahoo.com.br

Abstract

Reinforced concrete structures are essential for modern infrastructure. However, as classic concrete requires Portland cement, they can be a significant source of CO_2 emissions while facing challenges due to climate change and extreme events, putting their structural safety and users at risk. The effective performance of these structures depends on the steel-concrete (SC) bonding mechanism, and nanotechnology has shown promise for improving overall structural performance. In this sense, this study focuses on using carbon nanotubes (CNTs) to enhance the performance of Portland cement-based materials and reduce cement usage, aiming to meet safety, sustainability, and innovation demands. Precisely, this experimental research aims to (i) examine the effects of adding different CNT contents (0.025%, 0.05%, 0.075%, and 0.10% by weight of cement) on concrete's mechanical and physical properties; (ii) explore how bar diameter (d, 8 mm and 10 mm), roughness (plain and ribbed), and embedded length ($4d$, $5d$, and $5.6d$) affect the SC adherence; and (iii) determine if CNTs impact bond strength. Additionally, the study introduces a methodology to (iv) investigate using CNTs specifically around the rebar – focusing on critical regions that could optimize nanomaterial use while reducing material waste – and (v) evaluate the SC bond strength in reduced-cement concrete with and without CNTs. Lastly, based on the general equation, the research (vi) assesses whether incorporating CNTs can reduce the anchorage length. For this, the CNTs were dispersed in water and manually mixed into the concrete. Then, seventy cylindrical specimens (110 × 220 mm) and fifty-two cubic specimens (150 mm on each side) with centralized steel bars were produced to assess the concrete's properties and analyze the bond-slip behavior, respectively. Among the main conclusions, incorporating 0.05% CNTs into concrete significantly improved compressive (+8.0%) and tensile strength (+22.2%), reduced porosity and water absorption (-9.5%), and enhanced steel-concrete bond strength, particularly for larger diameter bars and longer embedded lengths (+33.0% in plain bars). This optimal CNT content balanced performance improvements with reduced cement use, enhancing structural durability and environmental benefits.

Keywords: Bond-slip behavior; Carbon Nanotubes; Cementitious Materials; Low-carbon materials.

1. Introduction

Reinforced concrete (RC) structures have shaped human history expansion, making the construction of bridges, buildings, and infrastructures possible. However, in the face of climate change and increasingly frequent extreme events, there is a growing need for projects that guarantee the safety and durability of these structures. Concrete, in particular, is one of the most widely used materials in the world [1]. Its production is associated with high CO_2 emissions. Construction and demolition waste (CDW) generation also represents a significant environmental problem [2]. Besides, ensuring the structural safety of these RC buildings requires constant attention, as failures can have devastating consequences [3]. With this in mind, the design of RC structures must at least consider the structural, environmental, and technological factors, which still involve several barriers to overcome.

Considering the structural point of view, several factors are involved in ensuring safety, including the bonding mechanism between the steel bars and the concrete. Parameters such as the rebar diameter, roughness, embedded length, and concrete type directly influence the adhesion behavior and, consequently, the ability to withstand loads and guarantee the structure's integrity [4]. Diverse research fronts aim to improve these bonding mechanisms, and the equations proposed by technical standards have been constantly tested and revised, with research in the literature proposing models for predicting bond strength under various conditions [5–7].

As for the environmental aspect, various trends have been studied to reduce the impact of concrete use. Materials with low carbon content are gaining ground, such as alternative cement (e.g., Portland limestone cement and polymeric cement) [8,9]. Recycled CDW aggregates, once considered just waste, are now regulated by some standards to replace natural aggregates partially [10]. Reinforcements such as natural fibers (e.g., ramie and bamboo fibers), synthetic fibers (e.g., polypropylene and polymeric fibers), and nanomaterials (e.g., graphene oxide and nano-silica) have been incorporated into cementitious composites to increase the strength and durability of structures, reducing the need for frequent repairs and demolition [11–13]. The decarbonization of the cement industry has also been a focus of study, as well as the development of more efficient production processes and eco-friendly materials with lower greenhouse gas emissions [14,15].

On the technological side, implementing innovations on an industrial scale faces significant challenges. Technologies such as 3D printing of concrete and Building Information Modeling (BIM), for instance, have transformative potential but require overcoming technical barriers (e.g., finding the ideal consistency, workability, and strength properties of the cementitious material for different applications) and economic barriers (e.g., integrating the software with existing systems in companies) to be widely adopted [16,17]. Incorporating these technologies could revolutionize the sector, but it requires continuous effort to overcome current limitations and make their practical application feasible.

Given this need to meet the demands of safety, sustainability, and innovation, this research was developed with nanotechnology as a crucial component. Among the materials investigated, carbon nanotubes (CNTs) stand out as promising for improving the performance of Portland cement-based materials. These nanomaterials are tube-shaped structures built from laminated carbon sheets one atom thick, classified as single-walled (SWCNTs) or multi-walled (MWCNTs), depending on the number of cylinders formed after synthesis [18]. Although CNT dispersion may slightly reduce flowability, their minimal dosage enhances concrete properties independently of the water-to-cement

ratio. With minimal dosage, CNTs offer significant performance improvements, economic feasibility, and reduced material usage, surpassing the benefits of alternative additives like clays or rust inhibitors. Moreover, extensive reviews by the authors have revealed that the application of CNTs still requires a complete understanding of their contribution to improving the steel-concrete (SC) bonding mechanisms, which are governed basically by mechanical interlocking, frictional resistance and, to a lesser extent, chemical bonding. Therefore, incorporating CNTs into the concrete may influence these factors [19].

It should be noted that CNTs tend to agglomerate due to their hydrophobic nature and strong van der Waals forces between them [20]. Therefore, the appropriate choice of CNT type, content, and dispersion technique is essential to avoid worsening the engineering properties of cementitious materials [21]. To address this issue, Reis et al. [22] evaluated several physical and mechanical properties of concrete with CNTs pre-dispersed in cement at contents of 0.05% and 0.10% by weight of cement (% wc). The results revealed that adding 0.05% CNT to the concrete reduced its porosity by up to 12% and increased the compressive and tensile strengths by up to 16% and 29%, in that order. These same authors compared the effectiveness of the dispersion technique used in their research (pre-dispersion of powdery CNTs in cement particles in an isopropanol medium) with others frequently used by researchers in isolation or in combination, such as mechanical stirring, magnetic stirring, surfactant addition, and sonication. For this purpose, the variations obtained in the properties of porosity, ultrasonic pulse velocity, and compressive and tensile strengths were considered. In summary, it was concluded that pre-dispersing powdered CNTs in cement particles is effective, but using CNTs in aqueous suspension with industrial dispersion is more straightforward, safer, and potentially more efficient, mainly for industrial production [22].

As SC bonding depends, among other factors, on the concrete type and its properties, it is expected that if CNTs improve the concrete's resistance, its bond strength will also be enhanced. Research has pointed in this direction. Hawreen and Bogas [23] demonstrated that adding CNTs to concrete can improve compressive strength and SC bond by up to 21% and 14%, respectively. Song et al. [24] showed that CNT contents of 0.10% and 0.15% wc increased maximum bond strength by 37.2% and 49.7%, respectively, and that bond strength varied with the cover-to-bar diameter ratio and CNT dosage. Besides, Arel et al. [25] found that increasing compressive strength, cover thickness, and curing time improves bond strength. It is also worth noting that tensile stresses are generated by the interaction of the concrete with the steel bar, i.e., when the bar is pulled out of the concrete, this axial load causes radial and shear stresses. Cracks are then formed, reducing the confinement and bonding capacity, possibly leading to two failure modes, the bar pull-out or the concrete rupture [26,27]. However, it should be highlighted that while the above studies and several other previous ones have explored SC bonding behavior, they have primarily focused on the effects of using different CNT contents, bar diameters, and embedded lengths. In contrast, they have not addressed the possibility of incorporating nanomaterials only near the rebar, the region where the first microcracks that initiate the loss of adhesion appear. Common methods, which distribute CNTs uniformly throughout the concrete, face scalability challenges for complex structures due to the difficulty of achieving consistent dispersion and performance in large volumes. Therefore, focusing on incorporating CNTs only around steel bars and in critical regions, such as beam-column joints with high reinforcement density, aims to enable more efficient and sustainable use of these high-cost materials. In other words, a targeted approach to areas prone to microcracks and stress concentrations would be interesting for

evaluating structural performance and possibly reducing material waste and environmental impact.

Furthermore, the need for more understanding of the simultaneous effects of reducing the amount of cement and incorporating CNTs into the concrete on the SC adherence mechanisms draws attention from an environmental standpoint. Habert et al. [28] stated that the construction sector is slow and risk-averse and, therefore, focused on minor improvements that could be achieved across the value chain, such as using supplementary cementitious materials and optimizing clinker content in cement. According to the authors, these marginal gains could reduce CO_2 emissions by up to 50% if all stakeholders are engaged. Li et al. [29], in turn, investigated CNTs cement-based grouting materials and found that adding CNTs and fly ash enhanced dynamic compressive properties by 10%–32% compared to plain cement, not only improving these material's dynamic behavior but also reducing the amount of cement used to their production. These studies show promising results for decarbonization in the construction industry. However, the field still needs a clearer understanding of CNT influence in conventional concrete without fillers, other additions, or a low packing factor, reflecting the microporous paste phase typical of practical applications.

Therefore, this manuscript proposes a unique approach to investigate the bonding of steel bars in concrete with CNTs (CNT–concrete) and reduced cement, considering all the contexts above, including structural, environmental, and technological aspects. Specifically, this experimental research aims to (i) study the effects of adding different levels of CNTs (0.025%, 0.05%, 0.075%, and 0.10% wc) to concrete on its compressive strength, tensile strength, static modulus of elasticity, porosity, pore size distribution, and water absorption; (ii) investigate the influence of bar diameter (d, 8 mm and 10 mm), roughness (plain and ribbed) and embedded length ($4d$, $5d$, and $5.6d$) on SC bonding behavior; and (iii) assess whether incorporating these same CNT contents into concrete has an impact on its bond strength. In addition to these specific objectives, a new methodology is introduced to (iv) address the possibility of using CNT–concrete only around the rebar and (v) assess the SC bond strength of reduced-cement concrete with and without added CNTs. Finally, this article (vi) uses the general equation of the anchorage length to check whether it could be reduced by incorporating CNTs into the concrete mix.

2. Experimental Program

2.1. Materials

Concrete was produced using Portland cement I 52.5 N (EN 197-1 [30]), fine siliceous sand (0/2 mm), coarse siliceous sand (0/4 mm), coarse siliceous gravel (4/8 mm), and superplasticizer (SP, Fluid Optima 100 type, CHRYSO® brand). Fig. 1 presents the particle size distribution curves of the aggregates [31,32].

The nanotubes used in this research are multi-walled type purchased from Nanocyl SA in Belgium [33]. They are synthesized through the chemical vapor deposition (CVD) technique and marketed under the commercial name AQUACYL™ AQ0303, a waterborne dispersion of 3 wt % of NC7000™ containing an anionic surfactant (Fig. 2). Their main characteristics are listed in Table 1.

Ribbed and plain bars of 400–600 MPa grade (Eurocode 2 [34]) were used for the pull-out tests, with one stress-strain diagram (until steel yields) illustrated in Fig. 3 and the main properties summarized in Table 2. The ribbed steel bars were tensile tested in a Universal Testing Machine (UTM, Instron brand, 50 kN capacity) [35], and the yield

strength obtained for 8 mm and 10 mm diameter bars was 523 MPa and 547 MPa, respectively. These diameters were chosen because previous research has indicated that any interference at the SC interface can influence the adhesion behavior of thin bars (diameters up to 10 mm) during tests [36]. In addition, the low frequency of studies on adherence in thin bars makes it doubtful to define other diameter-dependent parameters, such as the anchorage length [4].

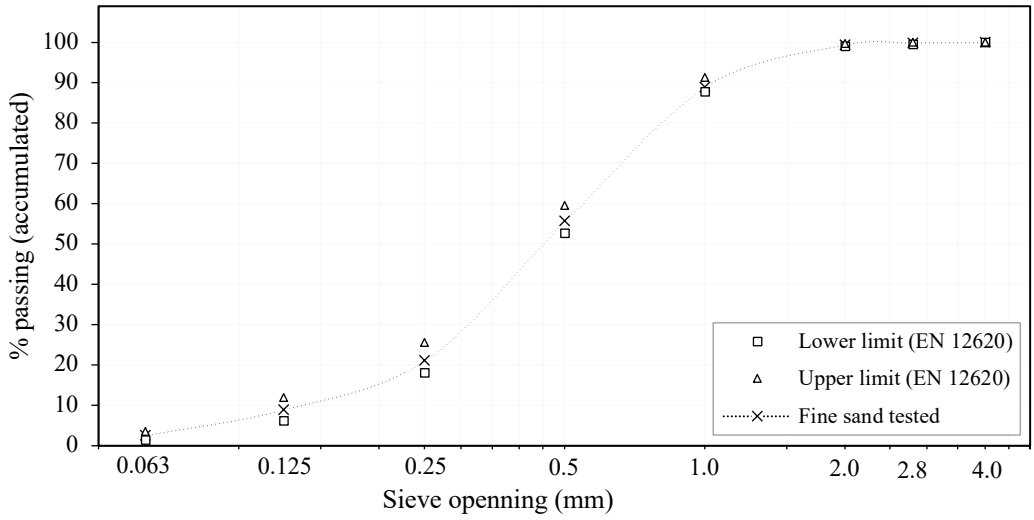

(a)

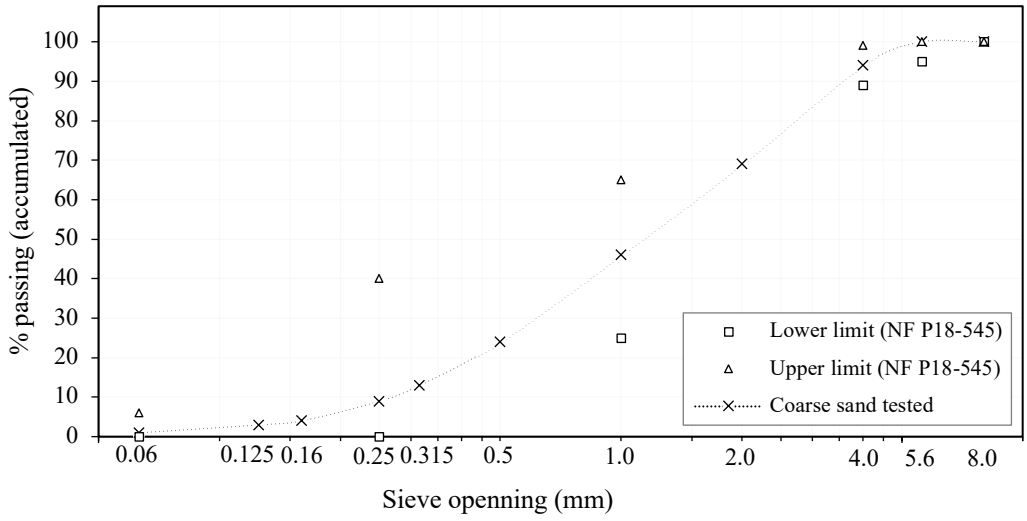

(b)

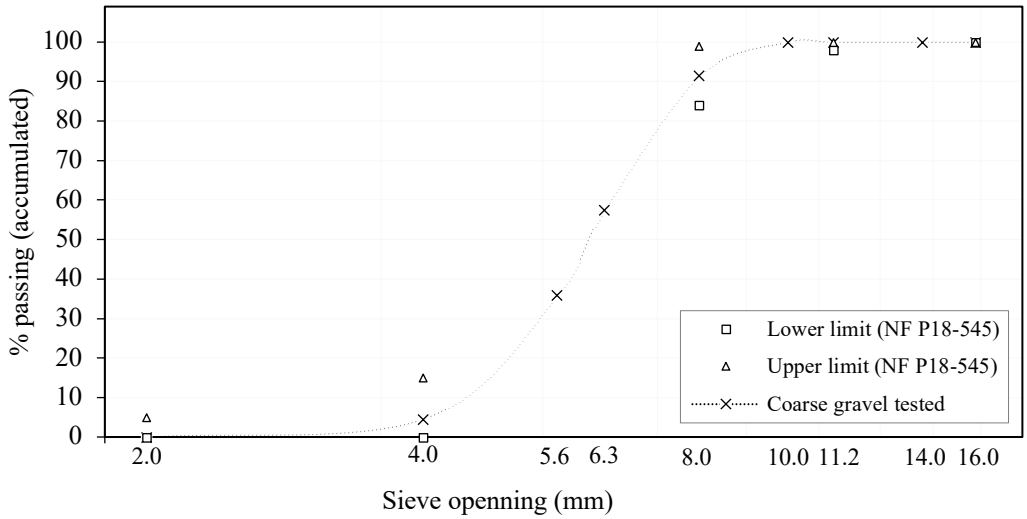

(c)

Fig. 1. Particle size distribution curves: (a) fine sand; (b) coarse sand; (c) coarse gravel.

(a) (b) (c) (d)

Fig. 2. MWCNTs: (a) Transmission Electron Microscopy image [37]; (b) gallon with 5 kg of AQ0303 (3 wt % NC7000 dispersion in water); (c) liquid dispersion aspect; (d) bucket with a solution containing CNTs dispersed in water after manual stirring.

Table 1. Characterization of the water dispersion (AQ0303) containing MWCNTs (NC7000) by the manufacturer [33,37].

Product	**Property**	**Value**
AQ0303 (aqueous dispersion)	pH	7–11
	Boiling point	100 °C
	Melting point	0 °C
	Viscosity after stirring at 25 °C	800–1000 cP
NC7000 (MWCNTs)	Average diameter [a]	9.5 nm
	Average length [a]	1.5 µm
	Surface are [b]	250–300 m^2/g
	Carbon purity [c]	90%
	Transition metal oxide [d]	< 1%
	Volume resistivity [e]	10^{-4} Ω.cm

Notes: Properties measured by: [a] Transmission Electron Microscopy; [b] BET Surface Area Analysis; [c] Thermogravimetric Analysis; [d] Inductively Coupled Plasma Mass Spectrometry; [e] Internal Test Method (resistivity on powder).

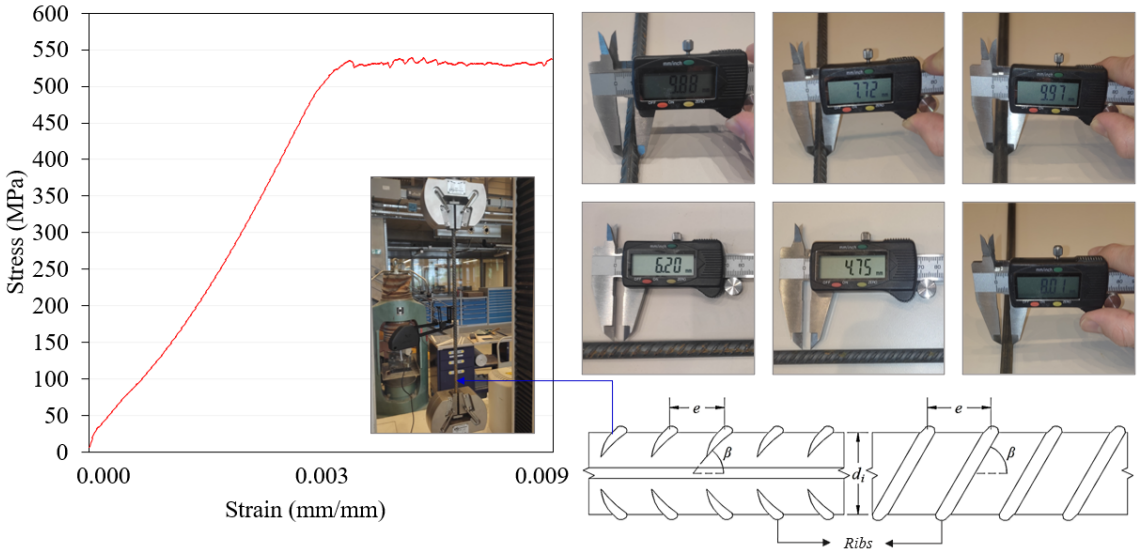

Fig. 3. Stress-strain curve (8 mm ribbed bar) and steel bar details.

Table 2. Steel bar dimensions.

Property or size	**Ribbed bars**		**Plain bars**	
Nominal diameter (d, mm)	8	10	8	10
Inner diameter (d_i, mm)	7.69	9.72	7.98	9.97
Rib height (h, mm)	0.90	0.92	–	–
Rib spacing (e, mm)	4.96	6.25	–	–
Rib inclination (β)	$\geq 45°$	$\geq 45°$	–	–

2.2. CNT dispersion

The CNTs were dispersed by mixing with water, followed by manual stirring. This method has already been tested in the literature and has led to satisfactory results, being reported as the simplest to replicate on an industrial scale [38,39]. Previous research by the authors has, therefore, indicated that it is valid as long as the CNTs are supplied in the form of aqueous suspension rather than powder [22]. Furthermore, this is the technique indicated by the manufacturer of the CNTs used in this study [33].

First, the amount of waterborne dispersion referring to a CNT content was calculated and weighed on a scale with milligram precision. For example, for a concrete sample whose manufacture requires 30 kg of cement, 7.5 g of CNTs are needed for the 0.05% CNT content, which corresponds to 250 g of waterborne dispersion with 3 wt % CNTs. Therefore, this CNT aqueous suspension was mixed with 50% of the water and manually stirred until the mixture was visually homogeneous and without clumps (Fig. 2d). This process was used on all the samples, regardless of the CNT content.

It is worth suggesting that further quantification methods, such as those used by Marcondes and Medeiros [40], who examined twelve different methods of dispersing MWCNTs in aqueous media based on three criteria – turbidity, the diameter of the agglomerates, and decantation – could be considered for future studies to assess the uniformity of the dispersion more accurately, as this study was limited to a visual inspection.

2.3. Mixture compositions and specimen production

Table 3 outlines the reference mix (C0, concrete without CNTs) prepared with 425 kg/m^3 of cement and a 0.42 water-to-cement ratio (w/c). This mix was obtained after performing a mixture rule and targeted an S3 slump class (100–150 mm) and a C60/75 compressive strength class (60/75 MPa for minimum characteristic cylinder/cube strength), according to EN 206-1 [41]. For the CNT–concrete samples, the maximum CNT content used was 0.10% wc—0.384 kg/m^3—following the authors' previous research recommendations [21,22]. Samples with CNT contents of 0.025% (C025), 0.05% (C05), 0.075 (C075), and 0.10% wc (C10) were prepared.

Besides, specimens containing C0 and C05 were also prepared in three equal layers (the one with C05 in the middle) as an initial attempt to optimize the use of the nanomaterial.

Lastly, reduced-cement concrete samples using 12% less cement without CNTs (LC0) and with 0.05% CNT (LC05) were also prepared using the same w/c (0.42). This reduction percentage was defined based on a previous preliminary study conducted by the authors with mortars, in which 0.05% CNTs were added to all samples and dispersed in the same manner described in the last section. The study aimed to determine a potential cement reduction that could be replicated in concrete. Different reduction percentages (0%, 5%, 10%, and 15%) were tested, and the main conclusion was that a reduction of up to 10% in cement content did not significantly compromise the mechanical properties of the mortar. However, workability was notably lost when the 15% cement reduction was applied, which could have been improved if some additive was used, leading to better results. Thus, the 12% reduction for the concrete samples was chosen as an intermediate value, balancing the potential for cement reduction with the preservation of workability and strength. Hence, the SP content was adjusted to a maximum of 1.4% wc to ensure the specified consistency.

Table 3. Concrete mix proportions.

Concrete	Cement (kg/m^3)	Water (kg/m^3)	Fine sand (kg/m^3)	Coarse sand (kg/m^3)	Coarse gravel (kg/m^3)	SP (% wc)
C0	425	180	280	485	990	1.2
LC0	374	158	280	485	990	1.4

2.4. Specimen production

Concrete production begins by adding a small quantity of water to moisten the inside surface of the concrete mixer (Eirich brand, 75-liter Model). The aggregates are mixed with 50% of the total mixing water for three minutes. Next, the cement, the remaining 50% of mixing water (with or without dispersed CNTs), and the superplasticizer are gradually added in this order. This blend is then mixed for an additional five minutes. Consistency is then measured by the slump test (EN 12350-2 [42]). Each composition is molded in two steps, filling half the volume each. The molds are then compacted on a vibration table for 10 seconds each.

For the samples containing CNT–concrete only around the bar, molding 150 mm-sided cubic specimens followed these steps: (i) batches of C0 and C05 were prepared simultaneously; (ii) a first layer of approximately 5 cm (1/3 of the specimen's height) was filled with C0; (iii) a second layer of approximately 2.5 cm (1/6 of the mold's height) was added using C05; (iv) the specimen was compacted on the vibration table for 10 seconds; (v) a new 2.5 cm layer was filled with C05; (vi) a final 5 cm layer was placed with C0; (vii) the specimen was compacted again for 10 seconds.

After 24 hours, all the samples are de-molded, wrapped in plastic, and left to cure at controlled temperature (20 ºC) for 28 days. Fig. 4 summarizes the process.

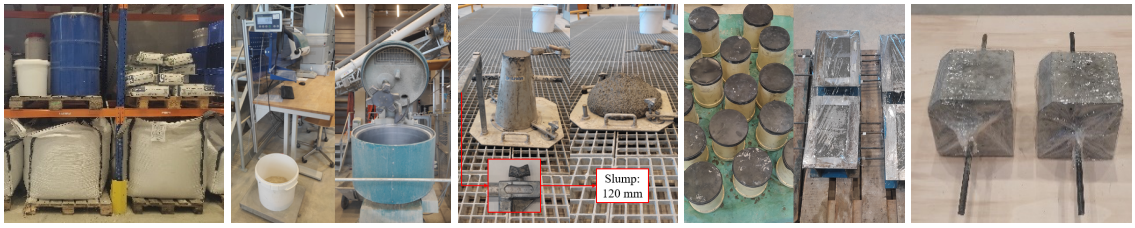

(a) (b) (c) (d) (e)

Fig. 4. Concrete specimens production process: (a) separating materials from stock; (b) weighing and mixing; (c) slump test; (d) casting; (e) curing after de-molding.

Seventy specimens measuring 110 × 220 mm (diameter × height) were produced using cylindrical plastic molds to measure the mechanical and physical properties. The two ends of the specimens were ground in a wet process on a grinding machine on the day of the tests. The properties studied were compressive strength, tensile strength, static modulus of elasticity (measured before the compression test with the same specimens), porosity, pore size distribution, and water absorption at 28 days, following the program listed in Table 4. Small pieces of the broken specimens were collected for porosimetric analysis.

Table 4. Mechanical and physical characterization test program.

Property	**Number of specimens**							
	C0	**C025**	**C05**	**C075**	**C10**	**LC0**	**LC05**	**Total**
Compressive strength and static modulus of elasticity	3	3	3	3	3	3	3	21
Tensile strength	4	4	4	4	4	4	4	28
Porosity and water absorption	3	3	3	3	3	3	3	21

Besides the specimens produced for the previous tests, fifty-two cubic specimens measuring 150 mm on each side were prepared using metallic molds to investigate SC bond behavior, following the setup in Fig. 5. These molds incorporate centralized holes through which the bar passes, ensuring its central positioning. The holes can adapt to bars of varying diameters. The maximum embedded length the molds can accommodate is 70 mm, as two small metallic tubes fixed inside the mold guarantee an isolated length of 80 mm (40 mm each). However, one can adjust the isolated length by attaching PVC tubes to the metallic ones, allowing for shorter bond lengths. Typically, the embedded length is positioned at the center of the specimen. Once the bar is in place, six screws, three on each side, are tightened to prevent the bar from shifting during vibration. Special attention ensures that, in the case of ribbed bars with equal embedded lengths, the bar has an equal number of ribs in contact with the concrete. Subsequently, a putty seals the tubes of the isolated length to prevent concrete from entering the tube, which could complicate demolding. With the setup complete, the molds are internally lubricated with oil, except for the steel bars. So, casting occurs transversely to the direction of the bar. Different diameters (d) and embedded lengths (l_b) of ribbed (R) and plain (P) bars were used, keeping the cover-to-bar diameter greater than five ($C/d > 5$) in all specimens to ensure the pull-out failure [43]. However, specimens of the C0 mix with ribbed bars ($d = 10$ mm, $l_b = 56$ mm) were tested, the bar rupturing instead of pulling out, so these

configurations were not considered in the CNT–concrete samples since greater resistance is expected in these cases. Instead, $l_b = 5d$ was used, the value recommended by the primary standards [44,45].

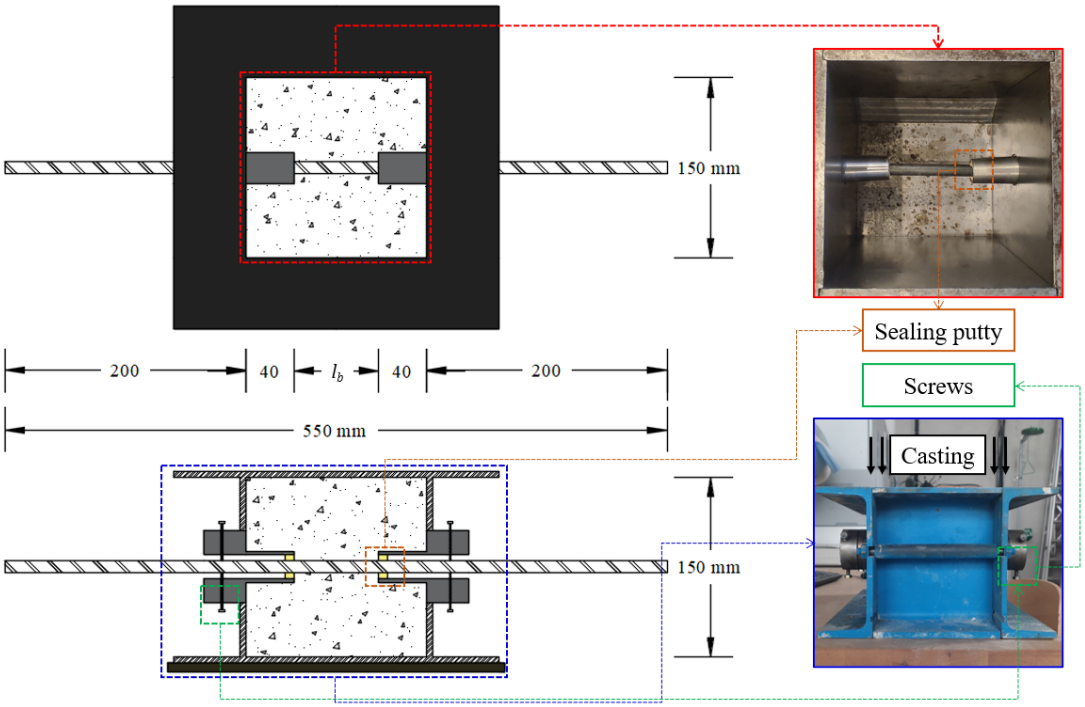

Fig. 5. Setup for producing pull-out test specimens.

Table 5 summarizes the corresponding test program, which included two specimens per group, except for C0/C05 (four samples), LC0 and LC05 (three samples each). It is worth mentioning that opting for small samples was supported by preliminary pull-out tests conducted with specimens cast on different days to account for production variability. On the first day, two batches (C_1 and C_2) were prepared, and four specimens were tested for each. On the second day, two additional specimens were produced for each batch. The results showed minimal deviation in the coefficient of variation (CV) of the maximum pulling force when reducing the sample size. For C_1, the CV was 3.95% with four specimens and 4.34% with two specimens, while for C_2, it was 4.21% with four specimens and 4.43% with two specimens. This consistency in load-slip behavior, even with fewer specimens, highlights the reliability of the results due to the high level of standardization achieved. Furthermore, many related studies use only two [46–48] or three [49–51] specimens, indicating that this approach aligns with established practices.

Table 5. Details of the pull-out test program.

Sample	Bar type	Concrete	d (mm)	l_b (mm)
C0-R-8-4	Ribbed	C0	8	32 ($4d$)
C0-R-8-5.6	Ribbed	C0	8	44.8 ($5.6d$)
C0-R-10-4	Ribbed	C0	10	40 ($4d$)
C0-R-10-5.6	Ribbed	C0	10	56 ($5.6d$)
C0-P-10-4	Plain	C0	10	40 ($4d$)
C0-P-10-5.6	Plain	C0	10	56 ($5.6d$)
C025-R-10-4	Ribbed	C025	10	40 ($4d$)
C025-R-10-5	Ribbed	C025	10	50 ($5d$)
C05-P-10-4	Plain	C05	10	40 ($4d$)

Sample	Bar type	Concrete	d (mm)	l_b (mm)
C05-P-10-5.6	Plain	C05	10	56 ($5.6d$)
C05-R-10-4	Ribbed	C05	10	40 ($4d$)
C05-R-10-5	Ribbed	C05	10	50 ($5d$)
LC0-R-10-4	Ribbed	LC0	10	40 ($4d$)
LC0-R-10-5	Ribbed	LC0	10	50 ($5d$)
LC05-R-10-4	Ribbed	LC05	10	40 ($4d$)
LC05-R-10-5	Ribbed	LC05	10	50 ($5d$)
C0/C05-R-10-4	Ribbed	C0/C05	10	40 ($4d$)
C075-R-10-4	Ribbed	C075	10	40 ($4d$)
C075-R-10-5	Ribbed	C075	10	50 ($5d$)
C10-P-10-4	Plain	C10	10	40 ($4d$)
C10-P-10-5.6	Plain	C10	10	56 ($5.6d$)
C10-R-10-4	Ribbed	C10	10	40 ($4d$)
C10-R-10-5	Ribbed	C10	10	50 ($5d$)

2.5. Experimental tests

2.5.1. Mechanical properties

The static modulus of elasticity test was performed according to EN 12390-13 [52], with the specimen's compressive strength ($f_{c,est}$) initially estimated from the concrete mix design. The cylindrical specimen was positioned within a strain gauge cage and centered on a 2500 kN MTS hydraulic press plate aligned along the machine's loading axis (Fig. 6a). The cage had three transverse strain gauges to measure radial deformations (Fig. 6b) and three displacement transducers to ascertain the average deformation across the measurement height. Through the control panel operated by a computer (Fig. 6c), a constant loading rate of 0.6 MPa/s was applied until the specimen reached a pre-load stress of 0.5 MPa, maintained for 20 seconds. Subsequently, the load increased to the upper limit stress ($\sigma_a = 0.3 f_{c,est}$), sustained for another 20 seconds before unloading to the lower limit stress ($\sigma_b = 0.1 f_{c,est}$). This cycle was performed three times and then the test was finished. Data acquisition software recorded the results, and the static modulus of the concrete specimen (E) was determined using Eq. (1), where ε_a and ε_b are the average strains corresponding to the σ_a and σ_b stresses, respectively.

$$E = \frac{\sigma_a - \sigma_b}{\varepsilon_a - \varepsilon_b} \quad (1)$$

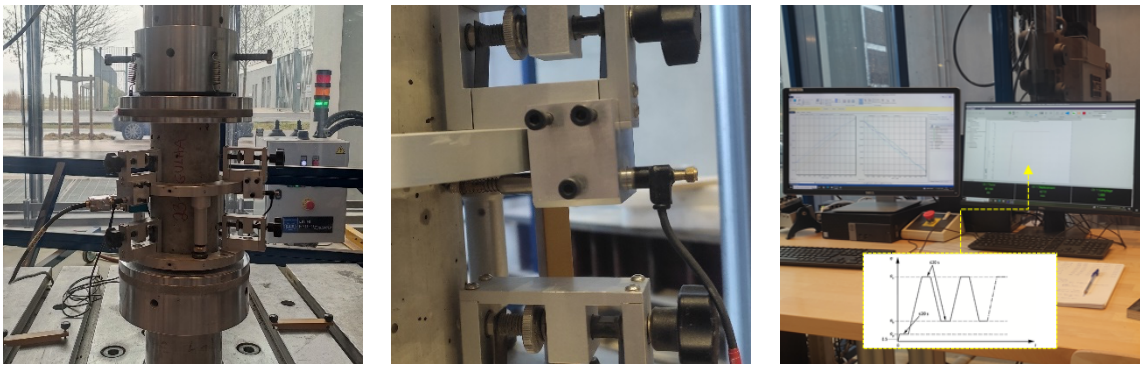

(a) (b) (c)

Fig. 6. Elastic modulus test setup: (a) specimen in the extensometer cage in the hydraulic press; (b) detail of the horizontal strain gauge sensor; (c) computers for data acquisition software and hydraulic press control panel.

Unbroken specimens, previously used for modulus of elasticity measurements, are subsequently tested for compressive strength (f_c or *CS*) on a Perrier UTM with a 2500 kN load capacity. This procedure follows the EN 12390-3 [53]. The concrete specimens were compressed at a consistent load rate of 0.6 MPa/s until maximum force (F) in Newtons. The UTM control panel displayed the outcomes, enabling the calculation of f_c using Eq. (2), where d represents the specimen diameter in mm.

$$f_c = \frac{4 \cdot F}{\pi \cdot d^2} \tag{2}$$

The splitting tensile strength by diametral compression ($f_{ct,sp}$ or *TS*) was measured using the same UTM in compliance with EN 12390-6 [54]. A compression load rate of 1.94 kN/s was applied until the specimen failed. The specimen was positioned horizontally over a metallic device. The maximum force (F) exerted on the specimen was recorded in Newtons on the UTM's control panel. Consequently, $f_{ct,sp}$ was calculated using Eq. (3), where L denotes the specimen length in mm.

$$f_{ct,sp} = \frac{2 \cdot F}{\pi \cdot d \cdot L} \tag{3}$$

2.5.2. Physical properties

The water absorption and porosity tests were conducted in line with ASTM C642-21 [55]. The procedure began by drying the specimen in an oven set to 110±5 °C for 72 hours (Fig. 7a). Afterward, the dry mass of the specimen (m_d) was determined using a precision weighing balance (Fig. 7b). The specimen was then submerged in water maintained at 21±2 °C for another 72 hours. After immersion, the saturated mass while still immersed in water (m_i) was measured with a hydrostatic balance (Fig. 7c). The specimen was removed from the water, its surface dried, and its saturated mass (m_{sat}) was recorded. The final step involved calculating the water absorption ($A_{(\%)}$) and the total porosity ($P_{(\%)}$) using Eq. (4) and Eq. (5), in that order.

$$A_{(\%)} = \frac{m_{sat} - m_d}{m_d} \cdot 100 \tag{4}$$

$$P_{(\%)} = \frac{m_{sat} - m_d}{m_{sat} - m_i} \cdot 100 \tag{5}$$

(a) (b) (c)

Fig. 7. Concrete physical characterization: (a) oven drying; (b) weighing after drying; (c) weighing on a hydrostatic scale.

The concrete's pore size distribution on a nanometric scale was measured by Mercury Intrusion Porosimetry (MIP) following the ISO 15901-1 standard [56] using an automatic mercury porosimeter (Micromeritics Autopore IV 9500, 414 MPa maximum pressure). The MIP method operates on the principle of applying pressure to force mercury into pores. As the pressure on the mercury increases, it can penetrate smaller pores. The pore size distribution can be determined by measuring the total volume of mercury that has entered the pores. Thus, fragments of concrete samples obtained from the mechanical tests, measuring approximately 1×1 (cm) and thoroughly dried in an oven, were subjected to low pressure (0.1 MPa) to allow the mercury to penetrate the larger pores of the sample. Subsequently, high pressures were applied (up to 414 MPa). The pore size distribution was then calculated using the Washburn equation (Eq. (6)) [57]:

$$d_p = \frac{4 \cdot \gamma \cdot \cos\theta}{p_c} \tag{6}$$

Where p_c represents the applied capillary pressure (MPa), d_p is the minimal pore diameter (μm) that mercury can enter at the pressure p_c, θ is the contact angle (º) between mercury and the pore surface (assumed to be 141.3° for cementitious materials), and γ is the surface tension of mercury (assumed to be 0.474 N/m).

2.5.3. Bond strength

The bond strength was measured through the pull-out test, whose setup is shown in Fig. 8. Before starting it, a few precautions were taken. It was checked that the adjusting platform and the support were level and firmly anchored to avoid unwanted movements. The specimen was then positioned on the adjusting platform, ensuring the steel bar was aligned correctly with the machine's traction axis. The end of the steel bar, not embedded in the concrete, was connected to the anchoring device, which is connected to the hydraulic jack. The load cell was attached between the steel bar and the hydraulic jack to measure the applied force. The displacement sensor was positioned to measure the steel bar's displacement about the concrete specimen accurately.

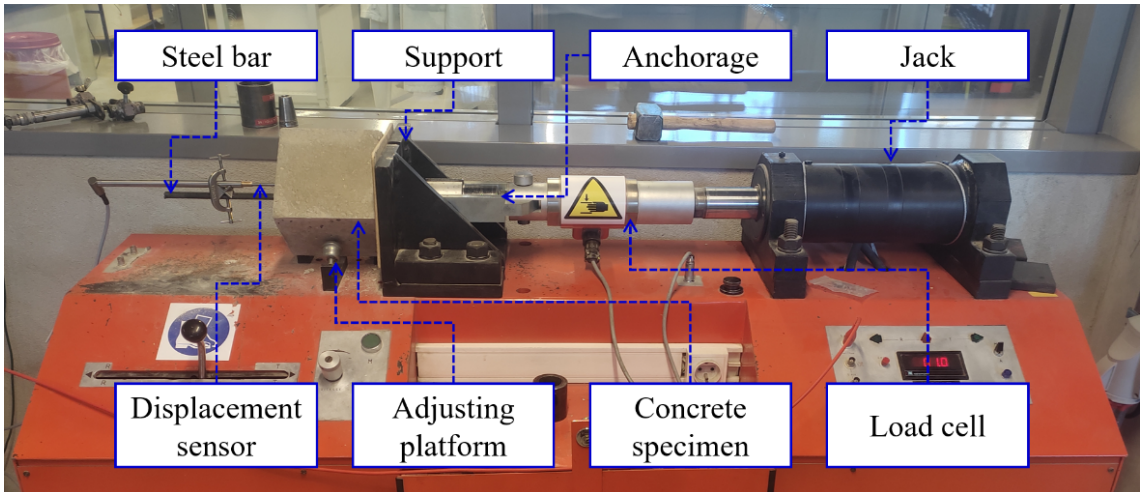

Fig. 8. Pull-out testing setup.

The test began with the hydraulic jack applying a tensile force to the steel bar. The force was applied gradually and controlled at a rate of $0.56d^2$ (N/s) [44]. During the load application, the sensors continuously monitored the force applied by the load cell and the displacement of the bar. This information was recorded automatically by a data acquisition system attached to the machine. The specimen's behavior was observed to detect any signs of failure, such as concrete cracks or steel bar slippage. The test was completed when the steel bar was effectively pulled out of the concrete or broke undesirably before pulling out. With the maximum pulling force (P) recorded in the test, the bar diameter (d), and embedded length (l_b), the maximum bond strength (τ_b) was calculated using Eq. (7). It should be emphasized that this equation assumes a perfect SC bond (which happens for zero or practically zero displacements when the mechanism is governed by chemical adhesion, which is very weak) and, consequently, that the bond stress is constant. Then, when the bar moves, this assumption is no longer valid, and the real value of τ_b is obtained, i.e., the use of P in this equation leads to the calculation of an equivalent rupture bond strength. In this research, τ_b will only be referred to as maximum bond strength for simplicity.

$$\tau_b = \frac{P}{\pi \cdot d \cdot l_b} \tag{7}$$

3. Results and Discussion

3.1. Concrete properties

Fig. 9 presents the *CS*, *E*, *TS*, $A_{(\%)}$, and $P_{(\%)}$ results, with the error bars on the graphs representing the standard deviation. Distinct letters indicate statistical differences between means as determined by the Tukey mean contrast test (5% significance), where A > B > C (and so on) and equal letters imply treatments with comparable mean values. The coefficient of variation (CV) was in the range of 1.44–5.79 for *CS*, 3.22–6.44 for *E*, 3.02–7.38 for *TS*, 0.90–2.72 for $P_{(\%)}$, and 1.01–2.94 for $A_{(\%)}$, all of them at 28 days.

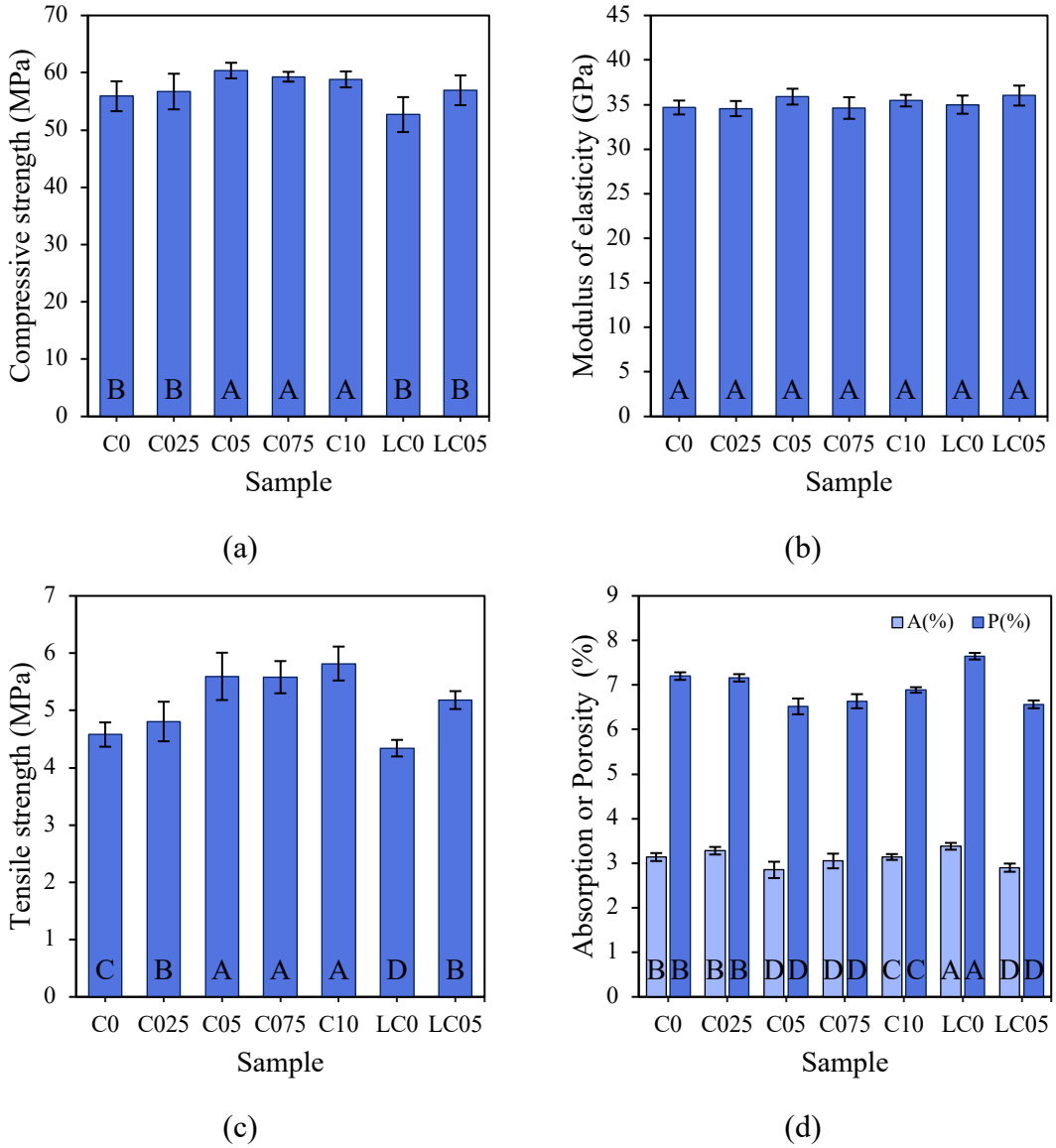

Fig. 9. Concrete properties results: (a) Compressive strength; (b) Modulus of elasticity; (c) Tensile strength; (d) Water absorption and porosity.

Fig. 9a shows that adding CNTs increased the samples' *CS* about the control mixture (C0). Still, the variation in relation to C0 was statistically significant only for groups C05 (+8.0%), C075 (+6.1%) and C10 (+5.3%). Considering the reduced-cement samples, there was a reduction in *CS* about C0 for the LC0 group (-5.3%) and an increase for LC05 (+1.9%), but these oscillations were statistically insignificant, according to the Tukey test. Comparing the LC05 mixture with LC0, an increase of 8.0% in *CS* was also noted. These results suggest that (i) incorporating CNTs into the mix tends to increase the *CS*, possibly because of their role as nucleation sites for cement hydration and filling nanopores, which makes the cement matrix more resistant and dense [58]; (ii) 0.025% CNT is not enough to affect *CS*, while 0.05% CNT is, and *CS* can be limited to this content as the results with up to 0.10% CNT were statistically equivalent; (iii) reducing the cement content tends to reduce the concrete's *CS* because it leads to fewer cementitious compounds (e.g., C–S–H) that contribute to the material's overall strength [59], but a 12% lower cement consumption did not have too many adverse effects on the performance of the concrete under compressive loading; (iv) the addition of 0.05% CNT

to the mix was enough to compensate for the reduction in *CS* due to the use of 12% less cement, as LC05 and C0 had comparable performances.

The results in Fig. 9b indicate that incorporating up to 0.10% CNT or reducing the cement content of the mix by up to 12% has no significant effect on the concrete's *E*, as the maximum variation was +3.87% (LC05). This statistical insignificance was confirmed by Tukey's test, which showed equivalent mean values for the *E* across all concrete samples produced in the study. It should be noted that the concrete's *E* is primarily influenced by the aggregate properties and the overall composite structure rather than minor variations in the binder content [60]. Moreover, these outcomes imply that the inclusion of CNT had a minimal impact on the concrete's stiffness under static loading, which is consistent with findings reported in the literature [61].

Fig. 9c, in turn, depicts the compelling effects of incorporating different levels of CNT, with an increase in *TS* in all cases. The variations were +5.0% (C025), +22.2% (C05), +21.9% (C075), and +27.1% (C10), with the *TS* of the last three groups being statistically equivalent. About the C0 group, the LC0 sample had a reduced *TS* (-5.2%), and the LC05 had an increased *TS* (+13.1%); about LC0, the *TS* of LC05 increased by 19.3%. These results (i) confirm that the role of CNTs is more effective in the behavior of concrete under tensile than compressive loading, which is due to their acting as tensile stress transfer bridges between the pores, delaying the propagation of cracks [24,62]; (ii) show that reducing the cement content by 12% also worsens the *TS*, but incorporating 0.05% CNT has a good effect, making it significantly higher than the sample with more cement and no nanomaterials (C0); (iii) suggest that using 0.05% CNT content can bring benefits by mitigating possible agglomeration problems reported in the literature when adding higher contents [38,63].

The results in Fig. 9d suggest the positive impacts of adding CNTs to the concrete's $P_{(\%)}$ and $A_{(\%)}$ and the adverse effects of reducing cement consumption. Sample C025 had its $P_{(\%)}$ reduced by less than 1.0% compared to C0, so 0.025% CNT was insufficient to produce a significant effect. On the other hand, in samples C05 and C075, the reduction was statistically considerable (-9.5% and -7.8%), resulting in the lowest $P_{(\%)}$ among the groups analyzed. Still, group C10 had a $P_{(\%)}$ 4.3% lower than the control group (C0). These variations suggest that the optimum CNT content to reduce both $P_{(\%)}$ and $A_{(\%)}$ is 0.05% wc. For the reduced-cement samples, reducing cement consumption by 12% increased $P_{(\%)}$ by 6.2% and $A_{(\%)}$ by 7.7% compared to the C0. When 0.05% CNTs were incorporated, however, there was a pronounced decrease in these properties, with the $P_{(\%)}$ of the LC05 sample being reduced by 8.8% compared to C0 and 14.1% compared to LC0 and reaching a similar value to the C05 one. This variation occurred because CNTs can refine the microstructure of the cement matrix, reducing the size and number of pores. Naturally, this improvement leads to lower permeability and water absorption [64,65].

Fig. 10 represents the pore size distribution of the concrete samples as the first derivative of the cumulative curve, $dV/d\text{Log}d_p$ (Log differential intrusion with data normalized per unit mass, mL/g) as a function of pore diameter (d_p). The labeled values in this figure correspond to each sample's most probable aperture (pore diameter). It depicts that the pore size distribution ranges mostly between 6 and 10,000 nm and reveals that CNTs mainly affect pores with a diameter of less than 1,000 nm. Group C0 had the most probable aperture equal to 349 nm. When CNT contents equal to 0.025%, 0.05%, 0.075%, and 0.10% wc were added, the d_p of samples C025, C05, C075, and C10 was reduced to 136 nm, 77 nm, 80 nm, and 83 nm, respectively. This finding supports the argument that CNTs can make the cementitious matrix denser by filling the pores of the C–S–H gel, as reported in the literature [66,67]. A similar effect can be seen in the curves of the LC0 and LC05 samples, whose d_p was reduced from 433 nm to 183 nm. It is worth

noting that the comparison of the C0 and LC0 samples confirms the adverse effect caused by the reduction in cement, as discussed above. Therefore, the results of the MIP tests carried out on small broken pieces of concrete (Fig. 10) validate the role of CNTs in improving the integrity of the cementitious matrix on a nanometric scale by preventing the displacement of microcracks and are in line with the $P_{(\%)}$ and $A_{(\%)}$ outcomes obtained from measurements using the entire specimen (Fig. 9d).

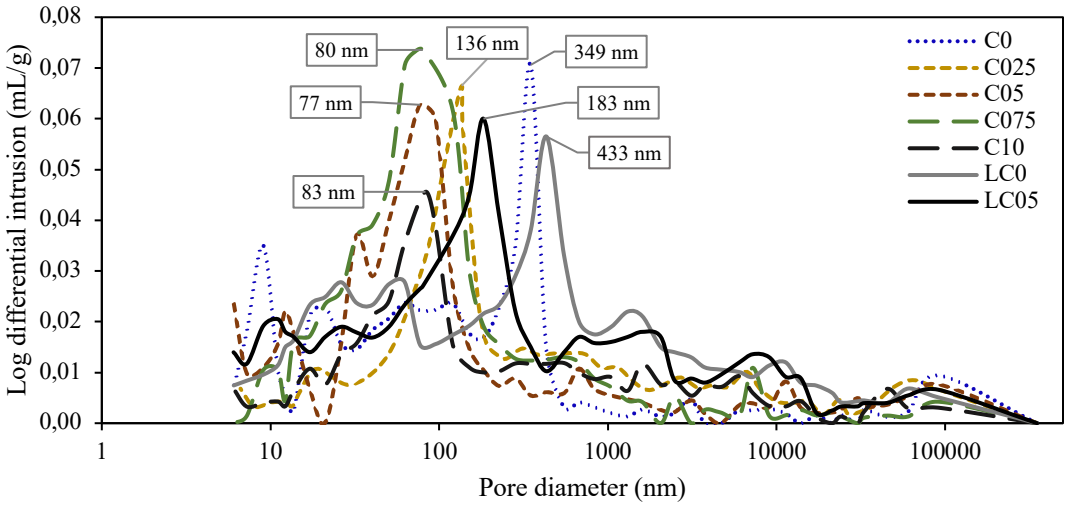

Fig. 10. Pore size distribution of the concrete samples.

Furthermore, these findings align with those from previous research conducted by the authors on a micrometric scale [22]. That study demonstrated that incorporating 0.05% CNT led to an increase in the proportion of pores with radii smaller than 250 µm and a decrease in the number of pores with radii greater than 750 µm, compared to the CNT–free sample. Consequently, the authors concluded that CNTs resulted in a concrete matrix with smaller, potentially less interconnected pores, which lowered its porosity and enhanced its strength [22].

The above results are noteworthy for studying the SC bonding behavior, especially those of *TS* and $P_{(\%)}$, as seen in the following subsection.

3.2. Bond strength and load-displacement relationship

Table 6 details the results of the pull-out test, namely: maximum pull-out load (P), maximum bond strength (or equivalent rupture bond strength, τ_b), displacement at peak force (ΔL_P), the ratio between the bond strength of the sample and that of the corresponding reference concrete ($\tau_b/\tau_{b,C0}$), the residual strength at 5 mm displacement ($\tau_{f,5mm}$), and the ratio between the residual strength and the maximum bond strength ($\tau_{f,5mm}/\tau_b$).

Table 6. Pull-out test results.

Sample	P **(kN)**	τ_b **(MPa)**	ΔL_P **(mm)**	$\tau_b/\tau_{b,C0}$	**Residual strength**	
					$\tau_{f,5mm}$ **(MPa)**	$\tau_{f,5mm}/\tau_b$
C0-R-8-4	31.89	39.65	0.43	1.00	21.48	0.54
C0-R-8-5.6	32.22	28.62	0.50	1.00	16.44	0.57
C0-R-10-4	43.73	34.80	1.00	1.00	20.16	0.58

C0-R-10-5.6*	49.51	28.14	0.68	1.00	–	–
C0-P-10-4	21.48	17.09	0.44	1.00	9.83	0.58
C0-P-10-5.6	27.46	15.61	0.09	1.00	5.69	0.36
C025-R-10-4	42.92	34.15	0.33	0.98	13.50	0.40
C025-R-10-5	46.43	29.56	1.58	1.05	13.71	0.46
C05-P-10-4	19.67	15.65	0.38	0.92	5.97	0.38
C05-P-10-5.6	36.51	20.75	0.07	1.33	12.59	0.61
C05-R-10-4	51.75	41.18	0.32	1.18	23.98	0.58
C05-R-10-5	57.06	36.32	1.61	1.29	23.28	0.64
LC0-R-10-4	45.97	36.59	0.97	1.05	19.41	0.53
LC0-R-10-5	48.03	30.58	1.44	1.09	20.70	0.68
LC05-R-10-4	51.19	40.73	0.58	1.17	28.48	0.70
LC05-R-10-5	52.35	33.32	0.58	1.18	19.56	0.59
C0/C05-R-10-4	36.02	28.66	0.43	0.82	17.15	0.60
C075-R-10-4	42.57	33.88	0.65	0.97	15.03	0.44
C075-R-10-5	52.85	33.65	0.52	1.20	20.91	0.62
C10-P-10-4	28.69	22.83	0.21	1.34	10.92	0.48
C10-P-10-5.6	30.53	17.35	0.19	1.11	7.77	0.45
C10-R-10-4	43.96	34.98	1.00	1.01	21.38	0.61
C10-R-10-5	45.60	29.03	0.92	1.03	14.64	0.50

Notes: All the data in this table represents the average of the results obtained on the treatment specimens (two specimens, except for C0/C05 with four samples and LC0 and LC05 with three samples); *The rebar ruptured before being pulled out.

In general, the highest τ_b occurred in sample C05-R-10-4 (41.18 MPa), a value 18% higher than the corresponding reference sample (C0-R-10-4), and it was also the sample with the lowest ΔL_P (0.32 mm). Among the reduced-cement concretes, sample LC05-R-10-4 had the highest τ_b (40.73 MPa), 17% and 11% more than the corresponding control samples, C0-R-10-4 and LC0-R-10-4. It is worth noting that this was the one with the best residual strength of all the groups (28.48 MPa), with 70% τ_b after 5 mm of sliding. These results indicate a positive effect of adding 0.05% CNT to the concrete, which increased the bond strength and delayed the onset of initial damage to the bond, suggesting greater durability of the SC bond. This same CNT content led to the greatest increases in τ_b in plain bars (e.g., 33% increase in sample C05-P-10-5.6), as well as helping to compensate for the loss of adherence associated with the 12% reduction in cement consumption in the reduced-cement concrete samples.

The following subsections discuss the influence of various factors on bonding behavior, with the pull-out load *versus* displacement curves ($P \times \Delta L$) representing the average results for each group at 28 days. It is worth noting that the pull-out tests were stopped when the displacement reached approximately 8 mm to preserve the integrity of the strain gauge sensor.

3.2.1. Influence of rebar diameter, roughness and embedded length

Fig. 11 presents the $P \times \Delta L$ curves to investigate the influence of the rebar diameter (8 mm and 10 mm), roughness (plain and ribbed), and embedded length ($4d$ and $5.6d$) on SC bonding behavior. For this purpose, using only the reference concrete (C0) was sufficient.

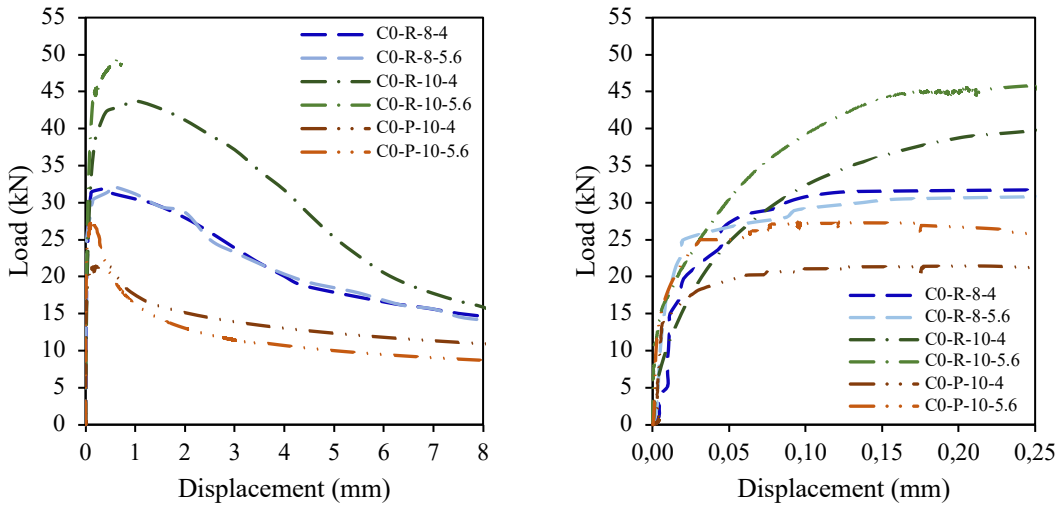

Fig. 11. $P \times \Delta L$ curves of concrete with different rebar diameters, roughnesses, and embedded lengths: (a) Global curve; (b) ΔL up to 0.25 mm.

The influence of diameter (d) was analyzed using the curves of the ribbed bar samples with similar embedded lengths (Fig. 11a). It was observed that a larger d (e.g., C0-R-10-4 × C0-R-8-4) provides greater pull-out force (P, 43.7 kN × 32.9 kN) and greater displacement at peak force (ΔL_P, 1.00 mm × 0.43 mm), i.e., greater capacity to absorb deformations before failure. Even so, it is worth mentioning that, keeping the cover-to-bar diameter ratio constant, larger diameter bars tend to cause more severe damage to the concrete when the specimen fails [68]. So, the results of this study were expected, as larger bars have a greater contact surface area, providing better stress distribution and greater stiffness, i.e., a more effective mechanical interaction between steel and concrete.

Roughness was evaluated by comparing samples of the same d and similar embedded lengths (l_b), as shown in Fig. 11a. Similar to the influence of using a larger d, it was noted that ribbed bars (e.g., C0-R-10-4 × C0-P-10-4) provide greater P (43.7 kN × 21.5 kN) and greater ΔL_P (1.00 mm × 0.44 mm). Research has shown that the bond stress-slip relationship remains stable for larger diameters (e.g., 16 mm) of plain steel bars in high-performance self-consolidating concrete with CS ranging from 40 to 90 MPa [69]. The present study indicated a similar trend for a smaller diameter (10 mm) in ordinary concrete, even for different embedded lengths, but not for ribbed bars. These outcomes were also foreseen, as ribbed bars have an increased contact surface due to the ribs and additional mechanical interaction.

Although expected, these findings were significant for evaluating the third parameter, the l_b, since its effect depends on the bar's d and roughness. For ribbed bars with a smaller d (8 mm), there was minimal variation attributed to the bond length (e.g., C-R-8-4 × C-R-8-5.6). The increased l_b did not lead to a noticeable increase in adhesion force. Still, it did allow for a slight increase in ΔL_P (Fig. 11b). For ribbed bars with a larger d (10 mm), a longer l_b resulted in a marked increase in bond strength (e.g., C0-R-10-4 × C0-R-10-5.6), leading to the bar breaking when the l_b was 5.6d. For the plain bars, a longer l_b increased the maximum P (e.g., C0-P-10-4 × C0-P-10-5.6), caused a pronounced reduction in ΔL_P, and failure was observed to occur quickly after the maximum bond strength was reached. These results are consistent with the literature [69]. Therefore, it can be stated that, generally, greater l_b increases the bond strength, the risk

of the bar breaking must be considered when increasing the l_b, and $P \times \Delta L$ curves for 8 mm bars indicate that the l_b has limited influence on this diameter.

This general analysis of the influence of rebar diameter, roughness, and embedded lengths, although not introducing novelties, can be helpful for further research, providing data to feed genetic, numerical, and artificial intelligence models that investigate SC bonding behavior. Particularly in this work, this analysis helped define the use of only one d (10 mm) and reduce the l_b from $5.6d$ to $5d$ in the case of ribbed bars, aiming the failure by pull-out and not by bar rupture, as mentioned above. The l_b of $4d$ remained in the following analyses to verify the possibility of using a lower value than that recommended by the primary standards ($l_b = 5d$), which could be valuable in elements with high reinforcement densification in RC structures.

3.2.3. Influence of CNT addition

Fig. 12 shows the $P \times \Delta L$ curves to study the effects of adding CNTs to concrete (contents up to 0.10% wc) on bonding behavior, with only 10 mm ribbed bars being used and the l_b set at $4d$. Fig. 13 is similar, differing only in the $l_b = 5d$. Fig. 14, in turn, contains $4d$ and $5.6d$ embedded lengths, but with plain bars instead of ribbed ones.

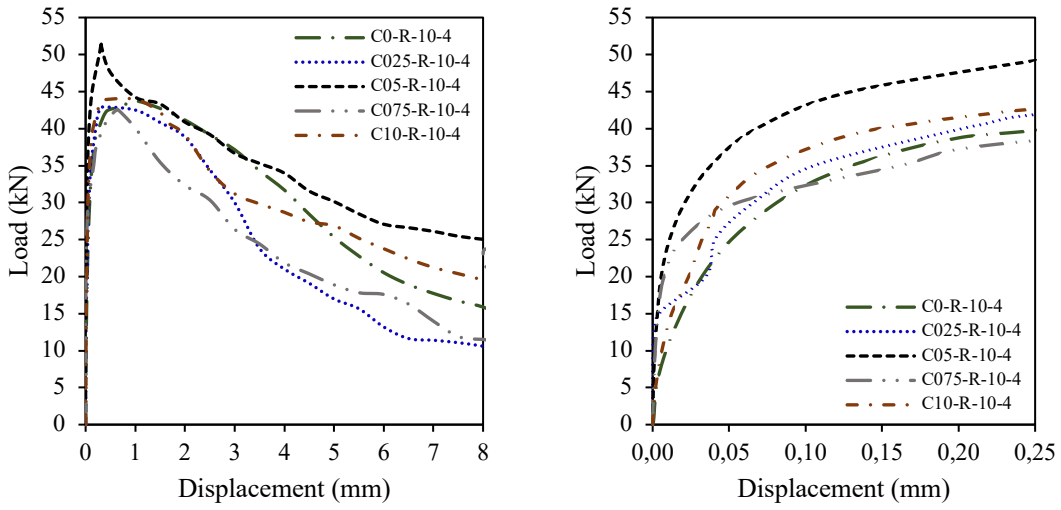

Fig. 12. $P \times \Delta L$ curves of concrete with 10 mm ribbed bars, $4d$ embedded length, and different CNT contents: (a) Global curve; (b) ΔL up to 0.25 mm.

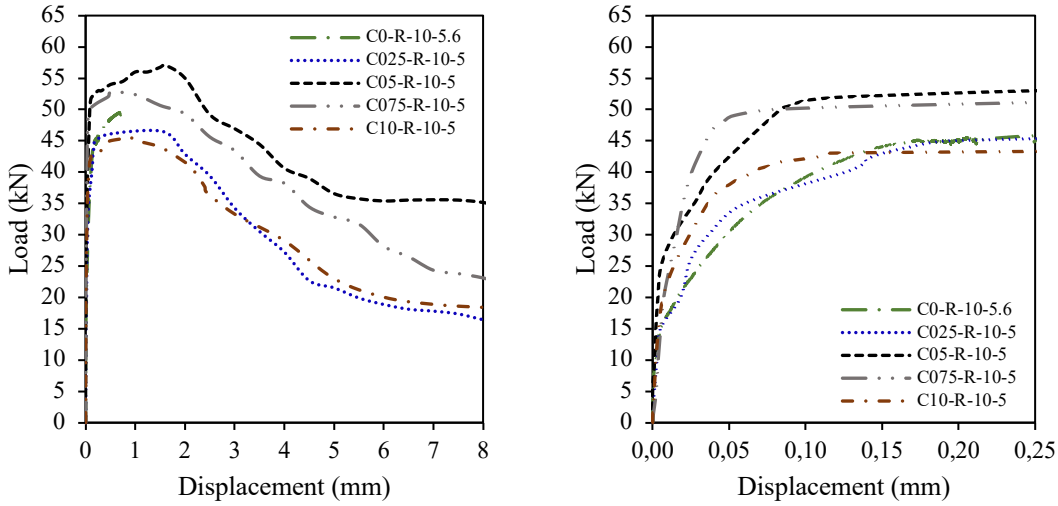

Fig. 13. $P \times \Delta L$ curves of concrete with 10 mm ribbed bars, $5d$ embedded length, and different CNT contents: (a) Global curve; (b) ΔL up to 0.25 mm.

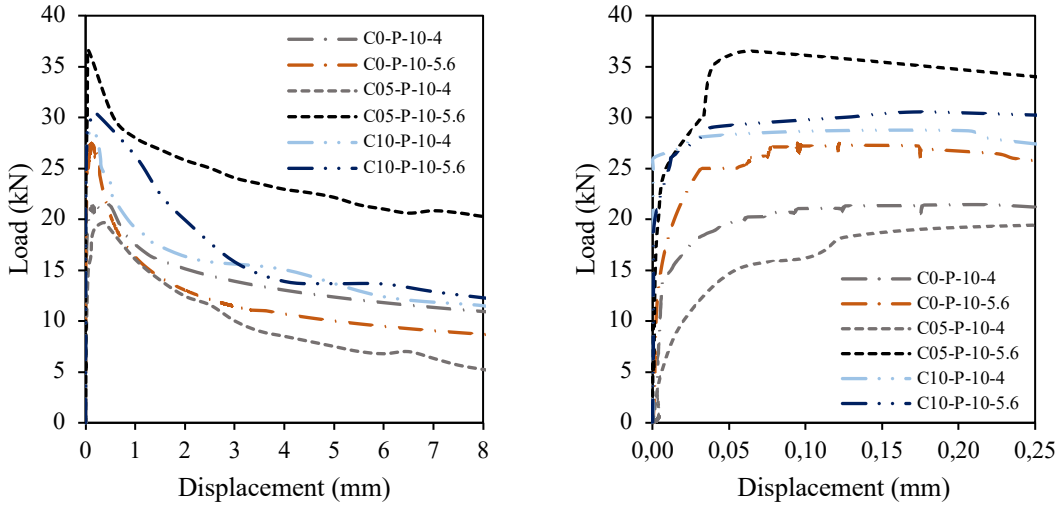

Fig. 14. $P \times \Delta L$ curves of concrete with 10 mm plain bars, $4d$ and $5.6d$ embedded lengths, and different CNT contents: (a) Global curve; (b) ΔL up to 0.25 mm.

Fig. 12a depicts that sample C05-R-10-4 is the only one that stands out, which is in line with the results of Table 6. Upon reaching the peak, the pull-out force suddenly decreases without maintaining the high levels for even a short distance after the peak. This occurrence may be related to the ribs' interlock, which slid more quickly when exceeded at high-stress levels. On the other hand, pull-out occurred more slowly in the other samples, with the C10-R-10-4 group peaking at a slightly higher value than the control group. Fig. 12b shows that the incorporation of CNTs reduced the pre-peak displacement in all the samples due to their higher compressive strength and lower porosity, which increased the packing of the material around the bars and consequently reinforced the bond strength.

When considering the curves in Fig. 13a, it can be seen that increasing the l_b to $5d$ resulted in a higher peak strength for sample C05-R-10-5, but, unlike in the previous

case ($l_b = 4d$), the post-peak behavior was not sudden. On the contrary, the maximum force was reached after more than 1.6 mm of displacement, indicating a greater capacity to deform without breaking. The adhesion behavior of groups C025-R-10-5 and C10-R-10-5 was very similar, although the compressive strength of the latter was higher. The C075-R-10-5 group performed well, somewhat like the C05-R-10-5, but with lower peak strength, residual strength, and pre-peak displacement (Fig. 13b). Studying the effect of CNT on the bonding mechanism of non-corrosive reinforcements to concrete, Taha et al. [70] observed that adding MWCNTs had an insignificant impact on the overall shape of the $P \times \Delta L$ curves for the bars tested but resulted in an increase in the normalized bond strength (e.g., +6.1% increase for 10 mm stainless steel bars). According to these authors, this fact indicates that CNT-concrete has a higher bond strength for the same *CS* class.

Fig. 14a, in turn, shows a pronounced effect of incorporating CNTs on the load-displacement relationship. When $l_b = 4d$, the highest peak force occurred in the C10-P-10-4 sample, notably higher than the C0-P-10-4 and C05-P-10-4 groups. When $l_b = 5.6d$, sample C05-P-10-5.6 showed the highest peak strength and also the highest residual strength. Groups C0-P-10-5.6 and C10-P-10-5.6 behaved similarly. Notably, all the groups with plain bars had a sharp drop after reaching the maximum bond strength since, without the influence of the bar ribs, the bond is controlled mainly by the friction between concrete and steel. From Fig. 14b, it can be inferred that, when using plain bars, it is more convenient to use the embedded length of $5d$ recommended by the primary standards [44,45] – even if they were not tested in this research – in concrete without CNTs than to reduce it to $4d$ and incorporate up to 0.10% CNTs into the concrete since the curves of the samples C0-P-10-5.6 and C10-P-10-5.6 are very similar; or, if higher bond strength is required, the embedded length can be increased to $5.6d$ or more, along with the incorporation of 0.05% CNT into the cementitious matrix. However, as these bars are less commonly used in reinforced concrete structures than ribbed ones, more attention should be paid to the latter.

Therefore, the results indicate that incorporating 0.05% CNT into concrete improves the SC adhesion, primarily in 10 mm diameter ribbed bars. With this addition, reducing the embedded length from $5d$ (recommended by the standards) to $4d$ while maintaining a higher bond strength is possible. The samples with CNTs had a higher maximum bond strength and lower pre-peak displacement due to the concrete's higher compressive strength and lower porosity, especially in the ribbed bars.

3.2.4. Influence of using CNT–concrete only around the bar

Fig. 15 depicts the $P \times \Delta L$ curves for analyzing the influence of incorporating CNTs only into the concrete surrounding the bar, using 10 mm ribbed bars and $l_b = 4d$ (C0/C05-R-10-4 samples). The results of similar samples but without the layer configuration were plotted for comparison purposes.

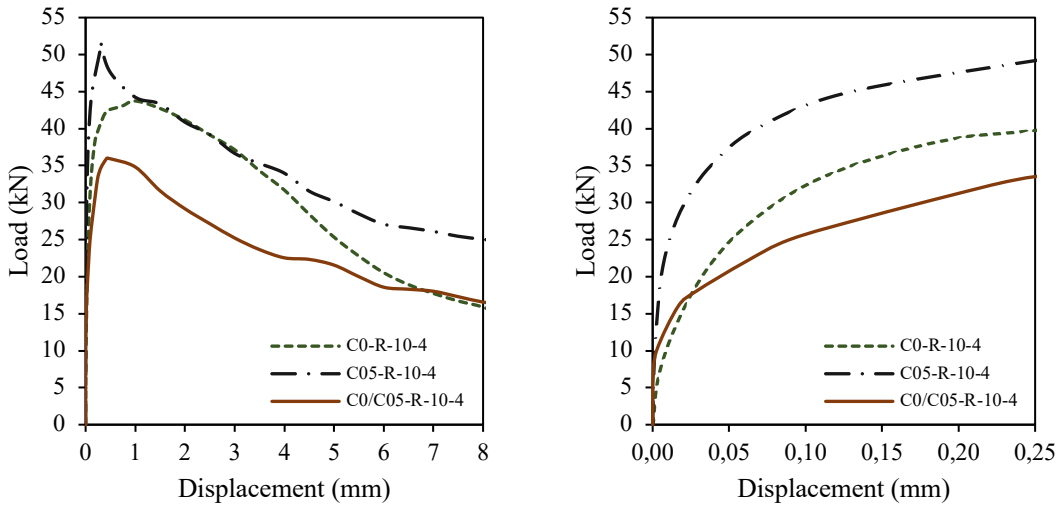

Fig. 15. $P \times \Delta L$ curves of concrete with 10 mm ribbed bars, 4d embedded length, and with CNT only in one layer around the bar: (a) Global curve; (b) ΔL up to 0.25 mm.

Fig. 15a shows that the proposal to use a CNT–concrete only around the rebar did not yield a good result. It can be seen that sample C0/C05-R-10-4 achieved the lowest peak strength, even lower than the reference sample (C0-R-10-4) and much lower than the one with CNTs throughout the specimen (C05-R-10-4). Fig. 15b indicates that the pre-peak behavior was relatively similar in the three samples but more irregular and with greater slippage at lower P levels in the one with the C0/C05-R-10-4.

Some factors may help explain this outcome. Although the two concretes (C0 and C05) had the same consistency at the time of casting, incorporating CNTs into one of them increased its strength and reduced its porosity. This fact means that the lower and upper layers of the specimen, filled with C0, may have provided less confinement to the central layer, composed of C05, and consequently to the steel bar.

In addition, even though the concretes with and without CNTs were mixed during densification, the vibration of the different mixtures may have resulted in a transition zone with inhomogeneous physical properties. This hypothesis is supported by similarities with the findings of Leeman et al. [71], who, although studying different concretes – conventionally vibrated concrete (CVC) and self-compacting concrete (SCC) – demonstrated that compaction has a significant influence on the porosity and width of the interfacial transition zone (ITZ). Specifically, CVC exhibited increased ITZ porosity and width compared to SCC, resulting in lower compressive strength, higher oxygen permeability, and greater water conductivity. Even though their study focused on different concrete types, the same principle may apply here: variations in the compaction of a sample containing two different batches could lead to localized inhomogeneities in ITZ properties. Furthermore, Leeman et al. [71] noted considerable differences in the porosity of the lower, lateral, and upper ITZ regions, emphasizing the importance of accounting for these variations in microstructural investigations. As such, this could help explain the potential formation of weak zones or discontinuities between the CNT and non-CNT mixtures, which may initiate structural failures under load. Complementary microstructural studies would be necessary to validate this hypothesis.

Another possible explanation is that different concrete mixes can have varying shrinkage rates and curing times. This circumstance can result in internal stresses and cracking at the interface due to incompatible volumetric properties during drying and

curing. Using shrinkage-reducing admixtures (SRAs) has been shown to mitigate these effects [72], and their combination with expansive additives can further reduce autogenous shrinkage and internal tensile stresses, improving dimensional stability [73]. However, no such admixtures were used in any of the concretes analyzed in this study, which may have led to more pronounced shrinkage rates and curing time differences between the mixes. These arguments further support the hypothesis established.

It should also be mentioned that there is an influence of the casting direction transverse to the steel bars (Fig. 5). As reported by Castel et al. [74], transverse casting can lead to the creation of small voids in the lower part of the bar, increasing porosity and reducing the area of contact between the concrete and the bar in this region. In related research, Eligehausen et al. [75] examined different failure modes of anchorage bars (pull-out, pull-out, and splitting) in normal-strength concrete. Various parameters, including the casting direction, were found to influence these failure modes. Similarly, previous studies have shown that casting orientation can impact the final flexural strength of ultra-high-performance fiber-reinforced concrete due to the preferential alignment of fibers along the casting direction [76]. Although all the specimens in the present research were manufactured under the same conditions, the approach used in this research could be better executed in molds that allow vertical casting. In other words, if casting were done in the same direction as the bar (preferably vertically), for example, by using a tube to isolate the two concretes before densification and enabling a more direct application of the CNT–concrete around the bar, there could be better confinement and adhesion, potentially improving the specimen's performance under the pull-out test.

With this perspective, the suggested approach would be interesting because CNTs (i) improve the tensile strength of concrete by acting as bridges for the transfer of tensile stresses, increasing the ability to withstand tensile forces and reducing the possibility of cracking and failure [77,78]; (ii) help control crack propagation by improving the toughness of concrete, which is crucial in tensile zones where the crack formation is more common [79,80]; and (iii) improve SC adhesion, resulting in better load transfer and greater structural efficiency, essential for the integrity of tensile regions. Thus, this topic can be considered for further investigation.

3.2.5. Influence of cement reduction

Fig. 16 presents the $P \times \Delta L$ curves to study whether reducing the amount of cement by 12% impacts the bonding of the steel bars to the concrete, as well as whether incorporating 0.05% CNT into this reduced-cement concrete has any effect on adhesion. For this purpose, 10 mm ribbed bars and $l_b = 4d$ were used. The embedded length equal to $5d$ was also tested, as shown in Fig. 17.

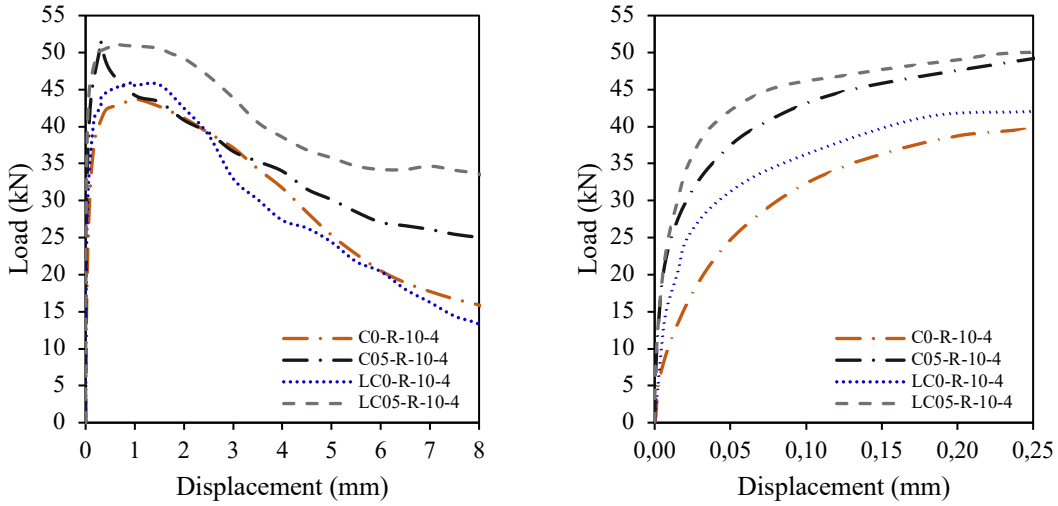

Fig. 16. $P \times \Delta L$ curves of reduced-cement concrete with 10 mm ribbed bars, 4d embedded length, with and without CNT addition: (a) Global curve; (b) ΔL up to 0.25 mm.

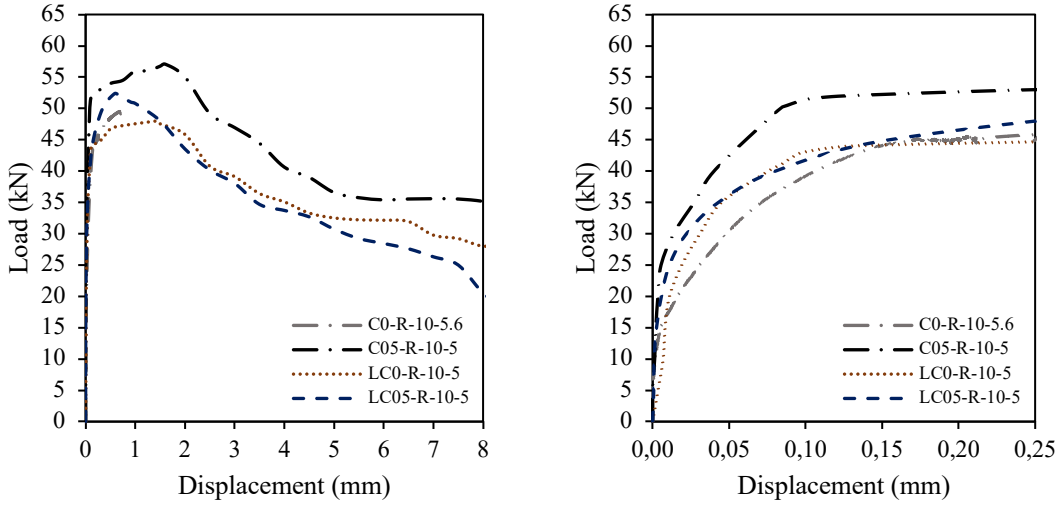

Fig. 17. $P \times \Delta L$ curves of reduced-cement concrete with 10 mm ribbed bars, 5d embedded length, with and without CNT addition: (a) Global curve; (b) ΔL up to 0.25 mm.

Fig. 16a shows that sample LC05-R-10-4 reached a slightly lower peak than C05-R-10-4 but had greater post-peak ductility and residual strength (Table 6), which, in a real case, could contribute to a less abrupt or more gradual collapse of the structure and reduce negative impacts. These results are associated with the microstructure of the concrete, as it was observed that by reducing the cement content and maintaining the 0.05% CNT, the sample showed greater homogeneity or pore size distribution and smaller pore diameter (Fig. 10), even though both have similar total porosity. It then led to a more behavior and a better stress distribution at the steel-concrete interface, delaying the complete rupture of the sample. It can also be seen that reference sample C0-R-10-4 had the lowest P, with a slightly lower peak than the reduced-cement reference sample, LC0-R-10-4. In general

terms, however, these two samples behaved very similarly. Fig. 16b shows that the ascending branch of the samples with CNTs is very similar to each other, i.e., in both cases, the CNTs contributed to reducing the pre-peak ductility by increasing the concrete strength and, consequently, improving the confinement of the bar.

When the l_b is increased from $4d$ to $5d$, the reduction in cement leads to different results. According to Fig. 17a, the peak strength of sample LC05-R-10-5 increased compared to sample LC0-R-10-5, but it was still lower and less ductile than C05-R-10-5. The latter, in turn, had higher residual strength. In addition, Fig. 17b shows that the ascending branch of the $P \times \Delta L$ curves was somewhat similar up to a 0.25 mm slip, except for sample C05-R-10-5, which had the highest P. Therefore, it can be inferred from these results that for $l_b = 4d$, the adherence had less influence from the concrete strength, governed mainly by the mechanical interlock of the ribbed bars. On the other hand, for $l_b = 5d$, the concrete strength began to govern the SC bonding behavior. In sample C05-R-10-5, for instance, the larger contact area improved stress distribution, and the higher TS and lower pre-peak ductility delayed the crack formation and propagation in the radial direction caused by the force P.

Considering the scenarios studied in this section and the results in Table 6, it can be seen that sample C05-R-10-5 achieved the highest P. From a structural point of view, a higher SC bond strength is essential to ensure the effective transfer of loads between the concrete and the rebars, increasing the structural capacity, stiffness, and durability of the construction and reducing cracking and premature failure of RC structures. From an environmental standpoint, it is known that the widespread use of cement to fabricate concrete is associated with significant CO_2 emissions into the atmosphere. In this investigation, reducing the cement content of concrete by 12% worsened SC bonding performance. In sample LC0-R-10-5, for instance, there was an imbalance between environmental benefits and the safety of structures. However, when this cement reduction was combined with CNT incorporation, there were gains in both terms since samples LC05-R-10-4 and LC05-R-10-5 performed better than the control ones. Precisely for these samples, using $l_b = 4d$ or $l_b = 5d$ led to similar P (51.19 *versus* 52.35 kN), but the shorter embedded length provided higher τ_b (40.73 *versus* 33.72 MPa) and higher residual strength after 5 mm of sliding ($0.70\tau_b$ *versus* $0.59\tau_b$).

In this sense, there is evidence that adding small CNT contents, e.g., 0.05% wc, can lead to lower consumption of steel bars and compensate for the reduction in cement by improving SC bond strength, reducing pre-peak ductility, and increasing residual strength. In other words, CNTs helped maintain the structural performance of the concrete, contributing to a reduction in cement consumption and, consequently, the associated CO_2 emissions.

3.3. Anchorage length

In the design of RC structures, the bond strength is crucial in determining the components' anchorage length. For longitudinal reinforcements, the sections to be respected must follow the guidelines provided in Eurocode 2 [34]. Based on the balance of forces along the embedded length (l_b) of the steel bar and assuming that the design stress of the bar at the position from where the anchorage is measured (σ_{sd}) – i.e., the design strength of the steel at the ultimate limit state, resulting from its yield strength (f_{yk}) divided by a safety coefficient (γ_s) usually equal to 1.15 (Eq. (8)) – must occur before bonding reaches maximum slip, the basic anchorage length ($l_{b,rqd}$) can be obtained from Eq. (9), in which f_{bd} is the ultimate bond stress, given by Eq. (10).

$$\sigma_{sd} = \frac{f_{yk}}{\gamma_s} \tag{8}$$

$$l_{b,rqd} = \frac{d}{4} \cdot \frac{\sigma_{sd}}{f_{bd}} \tag{9}$$

$$f_{bd} = 2.25 \cdot \eta_1 \cdot \eta_2 \cdot f_{ctd} \tag{10}$$

Where $\eta_1 = 1.00$ for good bond conditions; or $\eta_1 = 0.70$ for bad bond conditions, $\eta_2 = 1.00$ for $d < 32$ mm; or $\eta_2 = (132 - d)/100$, for $d \geq 32$ mm, and $f_{ctd} = 0.21 \cdot {f_{ck}}^{2/3}$ for concrete strength class up to C60/75. Accordingly, the design anchorage length (l_{bd}) can be calculated by Eq. (11).

$$l_{bd} = \sigma_1 \cdot \sigma_2 \cdot \sigma_3 \cdot \sigma_4 \cdot \sigma_5 \cdot l_{b,rqd} \geq l_{b,min} \tag{11}$$

Where σ_1 is a coefficient for the effect of the bar form assuming adequate cover, σ_2 for the effect of concrete minimum cover, σ_3 for the effect of confinement by transverse reinforcement, σ_4 for the influence of one or more welded transverse bars (diameter > $0.6d$) along l_{bd}, σ_5 for the effect of the pressure transverse to the plane of splitting along l_{bd} (see in Eurocode 2 [34]), and $l_{b,min}$ is the minimum anchorage length if no other limitation is applied, considering unfavorable hypothesis (compressed bar), according to Eq. (12).

$$l_{b,min} = \max\left[0.6 \cdot l_{b,rqd}; 10d; 100 \text{ mm}\right] \tag{12}$$

Finally, the anchorage length value to be considered for a bar is given by Eq. (13).

$$l_{bd} = \max\left[l_{bd}; l_{b,min}\right] \tag{13}$$

From these equations, if the physical and geometric characteristics of the steel bar are the same in practical design situations, l_{bd} will essentially depend on f_{bd}, which in turn can be influenced, among other factors, by the concrete's strength. Taking the τ_b results obtained experimentally in this research and using them instead of f_{bd} (estimated according to Eurocode [34]) in Eq. (9) as an example, it can be seen that incorporating 0.05% CNT content into the concrete could reduce l_{bd} by approximately 8%–23% (e.g., LC05 and C05 samples) for 10 mm diameter bars. This reduction could benefit specific building components, such as RC structural joints. Put differently, problems related to excessive crossing of steel bars at structural joints could be reduced or even solved by adding an optimum CNT content to the concrete, making it easier to form and improve the final quality of the RC structure.

4. Conclusions

This paper evaluated the concrete properties (*CS* – compressive strength, *E* – static modulus of elasticity, *TS* – tensile strength, $P_{(\%)}$ – porosity, and $A_{(\%)}$ – water absorption) and the SC bond-slip behavior considering different CNT contents (0%, 0.025%, 0.05%, 0.075%, 0.10% wc), cement reduction (12%), bar diameters (8 mm and 10 mm),

roughnesses (plain and ribbed), and embedded lengths ($4d$, $5d$, $5.6d$). The following conclusions can be drawn:

i. Incorporating 0.05% CNTs to concrete increased its *CS* by up to 8.0%, compensating for the reduction in strength caused by the 12% decrease in cement content while having no significant effect on its *E*. Adding 0.10% CNTs increased concrete's *TS* by up to 27.1%, with 0.05% CNT content improving *TS* even with a 12% reduction in cement content. In addition, the incorporation of 0.05% CNTs significantly reduced concrete's $P_{(\%)}$ and $A_{(\%)}$ by up to 9.5%, which could neutralize the adverse effects of cement reduction. Finally, CNTs reduced the diameter of pores, especially those smaller than 1,000 nm, making the cement matrix denser and improving its integrity. These findings indicate that using CNTs was beneficial compared to plain concrete, but the 0.05% CNT content was the optimal one for the properties studied, as higher amounts yielded statistically equivalent or less favorable results.

ii. Samples with larger bars (10 mm diameter), ribbed bars, and longer embedded lengths ($l_b = 5d$) had increased pull-out force and ability to absorb deformations in the concrete. However, the risk of rupture must be considered when raising the l_b, especially for larger-diameter ribbed bars, while for 8 mm bars, the l_b has little influence. This analysis can be helpful for future research and for feeding genetic, numerical, and artificial intelligence models that investigate the SC bonding behavior.

iii. Incorporating 0.05% CNT into concrete notably enhanced SC adherence, particularly for 10 mm diameter bars. This addition allows for reducing the l_b from $5d$ (as recommended by standards) to $4d$ while still achieving higher bond strength. The CNT–concrete samples exhibited greater τ_B and reduced pre-peak displacement, attributed to the concrete's increased *CS* and *TS* and lower $P_{(\%)}$, with the CNTs delaying the microcracks propagation, especially in the ribbed bars.

iv. Using CNT-concrete only around the steel bar was ineffective, resulting in lower ultimate strength and greater pre-peak slip than concrete with CNTs distributed throughout the specimen. The low performance of the proposed method can be attributed to the need for adequate confinement of the outer layers, inhomogeneity in the mixes' transition zone, and the influence of the direction in which the concrete is cast, which can increase porosity and create weak zones. Hence, a mold that allows the concrete to be cast in the same direction as the bar axis would be more effective. This approach could be considered in future research to examine further the potential of applying CNTs exclusively in the tensile regions of RC elements.

v. Reducing cement content while incorporating 0.05% CNTs resulted in a slightly lower peak pull-out force but improved post-peak ductility and residual strength, leading to a more gradual collapse and better stress distribution. This combination also enhanced the concrete's pore structure, increasing ductility and delayed rupture. Increasing the l_b from $4d$ to $5d$ showed that concrete strength began to influence bonding behavior, with the CNTs improving stress distribution and delaying crack propagation. Samples with 0.05% CNTs demonstrated that incorporating CNTs can enhance structural performance and reduce cement consumption, balancing environmental benefits with structural safety.

vi. Roughly speaking, incorporating 0.05% CNT into concrete could reduce l_{bd} by approximately 8%–23% for 10 mm diameter bars and $l_b = 5d$. This reduction

could benefit RC structural joints by alleviating issues related to excessive steel bar crossings, thereby improving the quality of the final RC structure.

These conclusions confirm that using nanotechnology to modification building materials, especially cementitious ones, can optimize the performance and durability of materials and structures. It can also contribute to the reduction of cement consumption and decarbonization, in line with the need to move towards a negative carbon impact and maximum efficiency in the production and use of building materials. It is worth noting that these findings are restricted to the parameters used in this research, i.e., CNT content of up to 0.10% wc, cement reduction of up to 12%, bar diameter of up to 10 mm, and embedded length of up to $5.6d$. Different parameters will require further research for a more comprehensive understanding.

Additionally, while preliminary pull-out tests showed minimal variability, a larger sample size would yield more robust conclusions. For future studies, analysis of variance via extrapolation (e.g., bootstrap simulations) is suggested to assess how confidence intervals might change with more specimens, mainly when a small sample size is unavoidable. Similarly, the morphological analysis of CNTs and tests such as Raman spectroscopy and X-ray Photoelectron Spectroscopy (XPS) would be welcome for providing a more detailed characterization of their structure and composition, contributing to understanding their interaction with other materials.

Acknowledgements

The authors thank Coordenação de Aperfeiçoamento de Pessoal de Nível Superior (CAPES, Finance Code 001), Fundação de Amparo à Pesquisa do Estado de Minas Gerais (FAPEMIG), Centro Federal de Educação Tecnológica de Minas Gerais (CEFET-MG), and Laboratoire de Mécanique Paris-Saclay (LMPS) for funding this research collaboration between Brazil and France.

References

[1] M. Wasim, A. Abadel, B.H. Abu Bakar, I.M.H. Alshaikh, Future directions for the application of zero carbon concrete in civil engineering – A review, Case Studies in Construction Materials 17 (2022) e01318. https://doi.org/10.1016/j.cscm.2022.e01318.

[2] H.C. Gomes, E.D. Reis, R.C.D. Azevedo, C.D.S. Rodrigues, F.S.J. Poggiali, Carbonation of Aggregates from Construction and Demolition Waste Applied to Concrete: A Review, Buildings 13 (2023). https://doi.org/10.3390/buildings13041097.

[3] M.F. Sulaiman, C.-L. Chin, C.-K. Ma, A.Z. Awang, W. Omar, The bond strength of reinforced concrete with confinement of recycled steel strap, J Clean Prod 369 (2022) 133352. https://doi.org/10.1016/J.JCLEPRO.2022.133352.

[4] E.D. Reis, R.C. de Azevedo, A.L. Christoforo, F.S.J. Poggiali, A.C.S. Bezerra, Bonding of steel bars in concrete: A systematic review of the literature, Structures 49 (2023). https://doi.org/10.1016/j.istruc.2023.01.141.

[5] B. Yang, K. Mao, J.H. Liu, K. Chen, M. Elchalakani, Modified regression model for bond-slip constitutive relationship between high-strength steel rebars and UHP-FRC based on experimental tests, Case Studies in Construction Materials 20 (2024) e02931. https://doi.org/10.1016/j.cscm.2024.e02931.

[6] V.M. de A. Monteiro, D.C.T. Cardoso, F. de A. Silva, B. Mobasher, The influence of steel fibers on the bond slip behavior between rebars and concrete: Experimental and analytical investigation, Constr Build Mater 411 (2024) 134357. https://doi.org/10.1016/j.conbuildmat.2023.134357.

[7] Y. Zhan, Z. Li, K. Chen, Y. Sun, Y. Li, F. Yue, W. Yang, Bond between 0.7-inch-diameter steel strands and UHPC: Pullout test, finite element simulation, and estimation of transfer length, Constr Build Mater 417 (2024) 135217. https://doi.org/10.1016/j.conbuildmat.2024.135217.
[8] M.A. Jungclaus, S.L. Williams, J.H. Arehart, W. V. Srubar, Whole-life carbon emissions of concrete mixtures considering maximum CO2 sequestration via carbonation, Resour Conserv Recycl 206 (2024) 107605. https://doi.org/10.1016/j.resconrec.2024.107605.
[9] M. Hasan Mizan, K. Matsumoto, Polymer cement mortar strengthened RC beams with/without silica fume as repair material, Constr Build Mater 409 (2023) 134046. https://doi.org/10.1016/j.conbuildmat.2023.134046.
[10] E.D. Reis, H.C. Gomes, R.C. de Azevedo, F.S.J. Poggiali, A.C.D.S. Bezerra, Bonding of Carbon Steel Bars in Concrete Produced with Recycled Aggregates: A Systematic Review of the Literature, C-Journal of Carbon Research 8 (2022). https://doi.org/10.3390/c8040076.
[11] S.C. Chin, I.G. Shaaban, J.P. Rizzuto, S.U. Khan, D. Mohamed, N.I.M. Roslan, A.A. Aziz, Predictive models for mechanical properties of hybrid fibres reinforced concrete containing bamboo and basalt fibres, Structures 61 (2024) 106093. https://doi.org/10.1016/j.istruc.2024.106093.
[12] G.W. Kim, H.-J. Choi, R. Piao, T. Oh, K. Koh, K. Lim, D.-Y. Yoo, Influence of hybrid reinforcement effects of fiber types on the mechanical properties of ultra-high-performance concrete, Constr Build Mater 426 (2024) 135995. https://doi.org/10.1016/j.conbuildmat.2024.135995.
[13] S.B. Nia, B. Shafei, Synergistic effects of nano and micro silica on fresh and hardened properties of self-consolidating concrete, Case Studies in Construction Materials 21 (2024) e03443. https://doi.org/10.1016/j.cscm.2024.e03443.
[14] J.V.S. Silva, E.D. Reis, R.C. de Azevedo, F.S.J. Poggiali, Towards eco-friendly cement-based materials: a review on incorporating oil shale ash, Discover Civil Engineering 1 (2024) 23. https://doi.org/10.1007/s44290-024-00027-5.
[15] H. Hafez, B. Malchiodi, N. Tošić, M. Drewniok, P. Purnell, A. de la Fuente, Decarbonization potential of steel fibre-reinforced limestone calcined clay cement concrete one-way slabs, Constr Build Mater 435 (2024). https://doi.org/10.1016/j.conbuildmat.2024.136847.
[16] N.O.E. Olsson, E. Arica, R. Woods, J.A. Madrid, Industry 4.0 in a project context: Introducing 3D printing in construction projects, Project Leadership and Society 2 (2021) 100033. https://doi.org/10.1016/j.plas.2021.100033.
[17] B. Ter Haar, J. Kruger, G. van Zijl, Off-site construction with 3D concrete printing, Autom Constr 152 (2023) 104906. https://doi.org/10.1016/j.autcon.2023.104906.
[18] K.M. Liew, M.F. Kai, L.W. Zhang, Carbon nanotube reinforced cementitious composites: An overview, Compos Part A Appl Sci Manuf 91 (2016) 301–323. https://doi.org/10.1016/j.compositesa.2016.10.020.
[19] E.D. Reis, H.F. Resende, P. Ludvig, R.C. De Azevedo, F. Spitale, J. Poggiali, A. Cesar, Bonding of steel bars in concrete with the addition of carbon nanotubes: A systematic review of the literature, Buildings 12 (2022) 1626. https://doi.org/10.3390/buildings12101626.
[20] M.S. Konsta-Gdoutos, P.A. Danoglidis, M.G. Falara, S.F. Nitodas, Fresh and mechanical properties, and strain sensing of nanomodified cement mortars: The effects of MWCNT aspect ratio, density and functionalization, Cem Concr Compos 82 (2017) 137–151. https://doi.org/10.1016/j.cemconcomp.2017.05.004.
[21] E.D. Reis, L.A. Borges, J.S.F. Camargos, F. Gatuingt, F.S.J. Poggiali, A.C.S. Bezerra, A systematic review on the engineering properties of concrete with carbon nanotubes, Journal of the Brazilian Society of Mechanical Sciences and Engineering 45 (2023). https://doi.org/10.1007/s40430-023-04117-w.
[22] E.D. Reis, H.F. Resende, A.L. Christoforo, R.M. Costa, F. Gatuingt, F.S.J. Poggiali, A.C.S. Bezerra, Assessment of physical and mechanical properties of concrete with

carbon nanotubes pre-dispersed in cement, Journal of Building Engineering 89 (2024) 109255. https://doi.org/10.1016/j.jobe.2024.109255.
[23] A. Hawreen, J.A. Bogas, Influence of carbon nanotubes on steel–concrete bond strength, Materials and Structures/Materiaux et Constructions 51 (2018). https://doi.org/10.1617/s11527-018-1279-8.
[24] X. Song, Q. Cai, Y. Li, C. Li, Bond behavior between steel bars and carbon nanotube modified concrete, Constr Build Mater 255 (2020). https://doi.org/10.1016/j.conbuildmat.2020.119339.
[25] H.Ş. Arel, Ş. Yazıcı, Ş. Yazici, Concrete–reinforcement bond in different concrete classes, Constr Build Mater 36 (2012) 78–83. https://doi.org/10.1016/j.conbuildmat.2012.04.074.
[26] K. Liu, J. Yan, X. Meng, C. Zou, Bond behavior between deformed steel bars and recycled aggregate concrete after freeze-thaw cycles, Constr Build Mater 232 (2020) 117236. https://doi.org/10.1016/j.conbuildmat.2019.117236.
[27] J.A. Bogas, M.G. Gomes, S. Real, Bonding of steel reinforcement in structural expanded clay lightweight aggregate concrete: The influence of failure mechanism and concrete composition, Constr Build Mater 65 (2014) 350–359. https://doi.org/10.1016/j.conbuildmat.2014.04.122.
[28] G. Habert, S.A. Miller, V.M. John, J.L. Provis, A. Favier, A. Horvath, K.L. Scrivener, Environmental impacts and decarbonization strategies in the cement and concrete industries, Nat Rev Earth Environ 1 (2020) 559–573. https://doi.org/10.1038/s43017-020-0093-3.
[29] G. Li, X. Shi, Y. Gao, J. Ning, W. Chen, X. Wei, J. Wang, S. Yang, Reinforcing effects of carbon nanotubes on cement-based grouting materials under dynamic impact loading, Constr Build Mater 382 (2023) 131083. https://doi.org/10.1016/j.conbuildmat.2023.131083.
[30] Comité Européen de Normalisation (CEN), EN 197: Cement – Part 1: Composition, specifications and conformity criteria for common cements, (2011) 30.
[31] Comité Européen de Normalisation (CEN), EN 12620 A1: Granulats pour béton, (2008) 59.
[32] Norme Française (NF). NF-P18-545, Granulats - Elément de définition, conformité et codification, (2021) 1.
[33] Nanocyl, AQUACYL™ AQ0303 - Multiwall carbon nanotube waterborne dispersions with ionic dispersant, Technical Data Sheet 2 (2023) 2–4.
[34] British Standard (BS), Eurocode 2: Design of concrete structures - Part 1-1: General rules and rules for buildings (EN 1992-1-1), The European Union 1 (2004) 230.
[35] Comité Européen de Normalisation (CEN), ISO 15630-1: Steel for the reinforcement and prestressing of concrete - Test methods Part 1: Reinforcing bars, rods and wire, ISO 15630 (2019) 24.
[36] E.P. Carvalho, E.G. Ferreira, J.C. da Cunha, C. de S. de S. Rodrigues, N. da S. da S. Maia, Experimental investigation of steel-concrete bond for thin reinforcing bars, Latin American Journal of Solids and Structures 14 (2017) 1932–1951. https://doi.org/10.1590/1679-78254116.
[37] Nanocyl. NC7000TM - Multiwall carbon nanotubes. Technical Data Sheet 2016:4.
[38] A. Hassan, H. Elkady, I.G. Shaaban, Effect of adding carbon nanotubes on corrosion rates and steel-concrete bond, Sci Rep 9 (2019). https://doi.org/10.1038/s41598-019-42761-2.
[39] A.V.S. Ribeiro, E.N. Guindani, P.J.P. Gleize, Analysis of Portland cement consumption reduction by using functionalized multiwalled carbon nanotubes in mortars, Revista IBRACON de Estruturas e Materiais 17 (2024) 1–11. https://doi.org/10.1590/s1983-41952024000200004.
[40] C.G.N. Marcondes, M.H.F. Medeiros, Análisis de dispersión de nanotubos de carbono en concretos de cemento Portland, Revista ALCONPAT 6 (2016). https://doi.org/10.21041/ra.v6i2.131.
[41] Comité Européen de Normalisation (CEN), EN 206: Concrete – Part 1: Specification, performance, production and conformity, (2000) 72.

[42] Comité Européen de Normalisation (CEN), EN 12350-2: Testing fresh concrete - Part 2: Slump test, (2019) 8.
[43] Comité Européen du Béton (CEB), CEB, fib Model Code Design Code 2010: Final Draft, Bulletin d'Information (2010).
[44] Comité Européen de Normalisation (CEN), EN 10080: Steel for the reinforcement of concrete - Weldable reinforcing steel - General, (2005).
[45] Réunion Internationale des Laboratoires et Experts des Matériaux (RILEM), Bond test for reinforcing steel: pull-out test, recommendation RC 6, Concrete Reinforcement Technology (1983).
[46] D. Li, R. Gravina, Y. Zhuge, J.E. Mills, Bond behaviour of steel-reinforcing bars in Crumb Rubber Concrete (CRC), Australian Journal of Civil Engineering 18 (2020) 2–17. https://doi.org/10.1080/14488353.2019.1680073.
[47] H. Wei, Z. Xiao, T. Wu, S. Zhao, W. Shen, Bond stress-slip properties and analytical models between high-strength lightweight aggregate concrete and high-strength steel bars, Constr Build Mater 454 (2024) 139110. https://doi.org/10.1016/j.conbuildmat.2024.139110.
[48] M. Zhao, G. Liu, L. Liu, Y. Zhang, K. Shi, S. Zhao, Bond of ribbed steel bar in high-performance steel fiber reinforced expanded-shale lightweight concrete, Buildings 11 (2021). https://doi.org/10.3390/buildings11120582.
[49] D. Shen, X. Shi, H. Zhang, X. Duan, G. Jiang, Experimental study of early-age bond behavior between high strength concrete and steel bars using a pull-out test, Constr Build Mater 113 (2016) 653–663. https://doi.org/10.1016/j.conbuildmat.2016.03.094.
[50] A. Qi, X. Liu, R. Xu, Y. Huang, Bond behavior of steel reinforcement in concrete containing ferronickel slag and blast furnace slag powder, Constr Build Mater 262 (2020) 120884. https://doi.org/10.1016/j.conbuildmat.2020.120884.
[51] Z.-Y. Huang, Y.-S. Huang, W.-Y. Liao, N.-X. Han, Y.-W. Zhou, F. Xing, T.-B. Sui, B. Wang, H.-Y. Ma, Development of limestone calcined clay cement concrete in South China and its bond behavior with steel reinforcement, Journal of Zhejiang University: Science A 21 (2020) 892–907. https://doi.org/10.1631/jzus.A2000163.
[52] Comité Européen de Normalisation (CEN), EN 12390-13: Testing hardened concrete - Part 13: Determination of secant modulus of elasticity in compression, (2021) 15.
[53] Comité Européen de Normalisation (CEN), EN 12390-3: Testing hardened concrete - Part 3: Compressive strength of test specimens, (2019) 20.
[54] Comité Européen de Normalisation (CEN), EN 12390-6: Testing hardened concrete - Part 6: Tensile splitting strength of test specimens, (2012) 11.
[55] American Society for Testing and Materials (ASTM), ASTM C642-21: Standard Test Method for Density, Absorption, and Voids in Hardened Concrete, ASTM (2021) 3.
[56] International Organization for Standardization (ISO), ISO 15901-1: Evaluation of pore size distribution and porosity of solid materials by mercury porosimetry and gas adsorption, Part 1: Mercury porosimetry, International Organization for Standardization (2016).
[57] E.W. Washburn, Note on a method of determining the distribution of pore sizes in a porous material, Proc Natl Acad Sci U S A (1921) 115–116.
[58] H. Ahmed, J.A. Bogas, M. Guedes, M.F.C. Pereira, Dispersion and reinforcement efficiency of carbon nanotubes in cementitious composites, Magazine of Concrete Research 71 (2019) 408–423. https://doi.org/10.1680/jmacr.17.00562.
[59] C. Hu, Y. Ruan, S. Yao, F. Wang, Y. He, Y. Gao, Insight into the evolution of the elastic properties of calcium-silicate-hydrate (C-S-H) gel, Cem Concr Compos 104 (2019) 103342. https://doi.org/10.1016/j.cemconcomp.2019.103342.
[60] D. Alfonso, M. Dugarte, J. Carrillo, C.A. Arteta, Effect of aggregate type on the elastic modulus and compressive behavior of concrete: A case study in Colombia, Constr Build Mater 411 (2024) 134131. https://doi.org/10.1016/j.conbuildmat.2023.134131.
[61] A. Hawreen, J.A. Bogas, Creep, shrinkage and mechanical properties of concrete reinforced with different types of carbon nanotubes, Constr Build Mater 198 (2019) 70–81. https://doi.org/10.1016/j.conbuildmat.2018.11.253.

[62] A. Carriço, J.A.A. Bogas, A. Hawreen, M. Guedes, Durability of multi-walled carbon nanotube reinforced concrete, Constr Build Mater 164 (2018) 121–133. https://doi.org/10.1016/j.conbuildmat.2017.12.221.
[63] S. Xu, J. Liu, Q. Li, Mechanical properties and microstructure of multi-walled carbon nanotube-reinforced cement paste, Constr Build Mater 76 (2015) 16–23. https://doi.org/10.1016/j.conbuildmat.2014.11.049.
[64] A.J.N. MacLeod, F.G. Collins, W. Duan, W.P. Gates, Quantitative microstructural characterisation of Portland cement-carbon nanotube composites using electron and x-ray microscopy, Cem Concr Res 123 (2019) 105767. https://doi.org/10.1016/j.cemconres.2019.05.012.
[65] M. Ramezani, Y.H. Kim, Z. Sun, M.M. Sherif, Influence of carbon nanotubes on properties of cement mortars subjected to alkali-silica reaction, Cem Concr Compos 131 (2022) 104596. https://doi.org/10.1016/j.cemconcomp.2022.104596.
[66] G. Liu, D. Kan, S. Cindy Cao, Z. Chen, Q. Lyu, Effect of multi-walled carbon nanotube on reactive powder concrete (RPC) performance in sulfate dry-wet cycling environment, Constr Build Mater 342 (2022) 128075. https://doi.org/10.1016/j.conbuildmat.2022.128075.
[67] M. Jung, J. Park, S. gul Hong, J. Moon, The critical incorporation concentration (CIC) of dispersed carbon nanotubes for tailoring multifunctional properties of ultra-high performance concrete (UHPC), Journal of Materials Research and Technology 17 (2022) 3361–3370. https://doi.org/10.1016/j.jmrt.2022.02.103.
[68] H. Zhang, H. Li, T. Lin, Z. Shen, Q. Feng, Experimental investigation on influence of embedment length, bar diameter and concrete cover on bond between reinforced bars and steel fiber reinforced concrete (SFRC), Case Studies in Construction Materials 21 (2024) e03742. https://doi.org/10.1016/j.cscm.2024.e03742.
[69] M. Dyba, Experimental study of bond-slip relationships in high-performance self-consolidating concrete with plain steel bars, Eng Struct 319 (2024) 118854. https://doi.org/10.1016/j.engstruct.2024.118854.
[70] A. Taha, W. Alnahhal, M. Irshidat, Effect of carbon nanotubes on the bonding mechanism of non-corrosive reinforcements to concrete, Structures 60 (2024) 105952. https://doi.org/10.1016/j.istruc.2024.105952.
[71] A. Leemann, B. Münch, P. Gasser, L. Holzer, Influence of compaction on the interfacial transition zone and the permeability of concrete, Cem Concr Res 36 (2006) 1425–1433. https://doi.org/10.1016/J.CEMCONRES.2006.02.010.
[72] A. Klausen, T. Kanstad, The effect of shrinkage reducing admixtures on drying shrinkage, autogenous deformation, and early age stress development of concrete, Structural Concrete 22 (2020) E596–E606. https://doi.org/10.1002/suco.201900583.
[73] M. Meddah, M. Suzuki, R. Sato, Influence of a combination of expansive and shrinkage-reducing admixture on autogenous deformation and self-stress of silica fume high-performance concrete, Constr Build Mater 25 (2011) 239–250. https://doi.org/10.1016/J.CONBUILDMAT.2010.06.033.
[74] A. Castel, T. Vidal, K. Viriyametanont, R. François, Effect of reinforcing bar orientation and location on bond with self-consolidating concrete, ACI Struct J 103 (2006) 559–567. https://doi.org/10.14359/16432.
[75] R. Eligehausen, R. Mallée, J.F. Silva, Anchorage in concrete construction, John Wiley \& Sons, 2013.
[76] K. Wille, G.J. Parra-Montesinos, Effect of beam size, casting method, and support conditions on flexural behavior of ultra-high-performance fiber-reinforced concrete, ACI Mater J 109 (2012). https://doi.org/10.14359/51683829.
[77] A.M. Rashad, Effect of carbon nanotubes (CNTs) on the properties of traditional cementitious materials, Constr Build Mater 153 (2017) 81–101. https://doi.org/10.1016/j.conbuildmat.2017.07.089.
[78] G. Liu, D. Kan, S. Cindy Cao, Z. Chen, Q. Lyu, Effect of multi-walled carbon nanotube on reactive powder concrete (RPC) performance in sulfate dry-wet cycling environment,

Constr Build Mater 342 (2022) 128075. https://doi.org/10.1016/j.conbuildmat.2022.128075.
[79] Y. Ruan, B. Han, X. Yu, W. Zhang, D. Wang, Carbon nanotubes reinforced reactive powder concrete, Compos Part A Appl Sci Manuf 112 (2018) 371–382. https://doi.org/10.1016/j.compositesa.2018.06.025.
[80] B. Han, Z. Yang, X. Shi, X. Yu, Transport properties of carbon-nanotube/cement composites, J Mater Eng Perform 22 (2013). https://doi.org/10.1007/s11665-012-0228-x.